Cu^{2+} tunable temperature-responsive Pickering foams stabilized by poly (N-isopropylacrylamide-co-vinyl imidazole) microgel: significance for Cu^{2+} recovery via flotation

Jiajia Xu[a], Huawei Qiao[a], Kai Yu[c], Mingfeng Chen[a], Canpei Liu[a], Walter Richtering[b], Huagui Zhang[a,b,*]

[a]College of Chemistry and Materials Science, Fujian Key Laboratory of Polymer Materials, Fujian Provincial Key Laboratory of Advanced Materials Oriented Chemical Engineering, Fujian Normal University, Fuzhou 350007, China

[b] Institute of Physical Chemistry, RWTH Aachen University, Landoltweg 2, 52056 Aachen, Germany, European Union

[c] School of Energy and Power Engineering, Jiangsu University, Zhenjiang 212013, China

Abstract：

Froth flotation has been a key chemical process extensively used in the recovery of heavy metal ions (e.g. Cu^{2+}) from contaminated water, while often criticized by a secondary pollution of the added collectors, and a less selectivity to specific ions since the ion removal by particles is independent from the post-step of particle flotation. To facilitate the industrial operation, a “smart” flotation with foams responsively stabilized after selective adsorption of target ions from competitive ions are highly desired. In the current study, “smart” foams stabilized by Cu^{2+} responsive microgels were presented as a proof-of-concept.

Firstly, a Cu^{2+}-responsive thermo-sensitive poly (N-Isopropylacrylamide-

co-Vinyl imidazole) (PNV) microgel with a hydrodynamic radius (R_h) ~ 334 nm and a fuzziness ~ 37.2 nm was synthesized. Cu^{2+}-imidazole complexation was demonstrated to enhance the microgel swelling with a softer and more homogenous microstructure, having the R_h increased by 30-50 nm for 0.005 M to 0.25 M Cu^{2+} and a significant volume phase transition temperature (VPTT) shift from ~ 40 ^oC to ~ 50 ^oC for 0.005 M Cu^{2+}, ~60 ^oC for 0.05 M Cu^{2+} and >> 60 ^oC for 0.25 M Cu^{2+}.

Secondly, temperature responsive foams with a ultra-stability below VPTT of the microgel and a rapid collapse above the VPTT were readily produced based on PNV microgels. Cu^{2+} complexation enabled a modulation of temperature responsiveness of the foams, able to maintain a good foam stability above a critical temperature (e.g. a life time > 6h at 45 ^oC for 0.25 M Cu^{2+}) where foams rapidly collapsed for other cations (e.g. ~2 min, ~10 min and ~15 min for Na^+, Mg^{2+}, Zn^{2+}, respectively), showing significance for selective recovery of Cu^{2+} from competitive ions.

Furthermore, an interfacial study at air-water interface revealed a better surface activity of Cu^{2+} -complexed PNV microgel with a less temperature dependence. An abrupt reduction of interfacial rheology around the VPTT with a G'_s(25 ^oC)/G'_s(70 ^oC) ratio ~300.1 observed was believed to be the main reason of the responsive foam destabilization for PNV2, which was avoidable by entanglements between Cu^{2+}-complexed PNV microgels, giving a G'_s(25 ^oC)/G'_s(70 ^oC) ratio ~1.68. Ultimately, the good Cu^{2+} selectivity of PNV2 microgel

was well demonstrated in mixed solutions of competitive ions Na^{+}, Mg^{2+}, Zn^{2+} in terms of Cu^{2+} sorption, particle swelling and foam stabillity. This study demonstrated a responsive Pickering foam stabilized by a Cu^{2+} tunable microgel, laying foundations to develop microgel-based flotation as a smart and green technology for Cu^{2+} recovery.

1. Introduction

Recovery of heavy metal ions from wastewater has been a worldwide concern in water remediation to address the indiscriminate discharge of industrial water into environment in the past decades [1, 2]. Because of its cheaper cost than noble metals, copper is widely and largely used in various fields ranging from electronics to biomedicines [3], and inevitably a large amount of copper ion (Cu^{2+}) contaminants are produced during the mining and processing of copper [4], being abundant in industrial effluents. It also can be detected at a high concentration in drainage fluids of acid mines, legacy mines and civil works, etc. [5, 6]. Being soluble in water while non-biodegradable and highly toxic in an excess concentration, the Cu^{2+} can accumulate in living organisms and pose an enduring toxic and carcinogenic effect to human [1, 7].

To remove Cu^{2+} from waste water, numbers of conventional water treatment techniques such as chemical precipitation [8, 9], adsorbent sorption [1, 10], electrochemical interactions [11, 12] and cementation [13], etc. have been reported in the literature, with each having its limitations. For example, the

electrochemical methods, though showing a certain selectivity and efficiency, are limited by its difficulty of scale-up and the high energy input[12]; the chemical precipitation and cementation methods often require additional chemicals[13], which easily generating secondary wastes. Adsorbent sorption is generally considered as the most convenient and effective method due to its easy operation and high efficiency, with its maximum sorption capacity varying from few mg/g to tens or even hundreds mg/g, depending on the adsorbent materials[1]. However, the high efficiency of the adsorbents, mostly in states of nano-/micro-particles, is often compromised by difficulties of recovering the adsorbents from liquid, hence causing a secondary pollution. An independent post-treatment process of liquid-solid separation thus required in methods of adsorbent sorption and chemical precipitation, etc. makes the whole treatment system complex, costly and difficult to be scaled up for practical applications.

Froth flotation, originating from mineral mining, has become an important method to remove heavy metal ions from wastewater thanks to its low cost and easy scale-up [14]. The process is often implemented by first either precipitating the ionic metal species or uptaking the target ions with particulate adsorbents, then imparting the precipitates or particles hydrophobicity with frother/collectors (surfactants) to be attached to rising air bubbles and separated from water [15]. Also, there are flotation processes having collectors to interact directly with ions for recovery, also named “ion flotation”, which has been widely used for treatment of different heavy metal ion such as Cu^{2+} [15], Ni^{2+}, Zn^{2+}, etc.[16] by

selecting proper collectors. However, similar to most of conventional water treatment methods, the addition of surfactants and/or precipitants in flotation can cause a secondary pollution. Meanwhile, the processes of ion adsorption by particles and particle flotation are two operation units working independently with either less selective to the target ion, making the whole separation efficiency be low.

In this concern, a green responsive flotation process free of surfactant and can be "switched-on" by the pre-step of selective ion uptake would be of great value for the heavy metal ion recovery. For the sake, the current study aims to developing a Cu^{2+} tunable thermosensitive Pickering foam based on a Cu^{2+} responsive microgel, as a potential fundamental study for future design of a responsive flotation for green and selective Cu^{2+} recovery.

To meet the objectives, the design of Cu^{2+} responsive microgels and the understanding of the “smart” foam stabilization/destabilization mechanism are the keys. Pickering foams, having particles irreversibly anchored at the gas-liquid interface with an extremely large detachment energy and an interfacial film being formed with strong mechanics, are considered to be ultra-stable[17]. To make the foam “smart” with stability switchable at will between stable and unstable states, stabilizers responsive to external stimuli (e.g. pH, temperature and ionic strength, etc.) are often employed [18].

Microgel, a self-adaptable three-dimensional cross-linked polymeric colloidal particle that can swell and soften by up-taking large amounts of solvent,

represents one of the most interesting stimuli-responsive emulsion stabilizers [19, 20], while scarcely reported to stabilize foams [21]. In particular, chemically cross-linked poly(N-Isopropylacrylamide) (pNIPAM) particle, first reported in 1986 [22], is one of the most popular microgel systems of study as responsive emulsion/foam stabilizer, thanks to its thermo-sensitivity having a volume phase transition temperature (VPTT) ~ 32 ^{o}C. Below the VPTT particles swell as a result of the strong hydrogen bonding between the amide groups in pNIPAM chains and water, and above the VPTT the particles de-swell as a result of water expelling from the macromolecules [23-29]. In addition, most of the pNIPAM-based microgels are non-toxic and environment-friendly, gaining applications in broad fields. Note that there are also some newly emerging microgels designed and fabricated from natural sources such as nanocellulose for the use as soft stabilizer of Pickering emulsions/foams [30].

In the myriad of responsive emulsions stabilized by microgels [31], both emulsions stabilized by swollen microgel while destabilized by microgel de-swelling [31, 32] and those with reversed stability by de-swollen microgels while destabilized by particle swelling have been reported [33, 34]. Though various explanations have been proposed for the stimuli-responsive destabilization of microgel stabilized emulsions including reduction in interfacial coverage area, desorption of microgels from the interface and change of interfacial viscoelasticity, etc. upon deswelling/swelling of the microgels at the interface, the exact underlying mechanisms still remain a matter of debate [35-38].

On the other hand, pNIPAM-based microgels or hydrogels copolymerized with metal-receptor ligands, such as nitrogen-based ligands [39, 40] and crown ether-based ligands [41, 42], have been prepared for design of indicators, chemosensors or adsorbents to detect, discriminate or adsorb specific metal ions according to the metal ion binding to ligands. Notwithstanding the great significance of ion-ligand complexation in water treatment [43], ion-responsive microgels are rarely used for producing “smart” emulsions or foams to be tunable by specific metal ions, let alone looking into the underlying “smart” control mechanism and their potential applications.

In this study, 1-vinylimidazole(VIM) was introduced as a comonomer to copolymerize with NIPAM to prepare a thermosensitive ionic microgel p(NIPAM-co-VIM) (abbreviated as PNV) via surfactant-free precipitation polymerization. The VIM comonomer was not only expected to alter the size, swelling property and surface activity of microgel, but more importantly the imidazole group of VIM is a ligand widely used to chelate Cu^{2+} [44]. The microstructure of PNV microgels regarding Cu^{2+} complexation effect was studied via light scattering. “Smart” foams with a clear temperature responsiveness of stabilization/ destabilization were simply prepared by PNV microgels and the effect of Cu^{2+} complexation was studied in comparison to other cations. Moreover, interfacial behavior of the microgels at air-water interface was investigated using pendant-drop analysis and surface shear rheology to reveal the underlying responsive foam destabilization mechanisms.

2. Experimental

2.1. Chemicals

N-Isopropylacrylamide (NIPAM), N, N'-methylenebisacrylamide (BIS), 1-vinylimidazole (1-VIM), 2,2-azobis (2-methylpropionamidine) dihydrochloride (AIBA), copper sulfate ($CuSO_4 \cdot 5H_2O$), zinc sulfate ($ZnSO_4$), magnesium sulfate ($MgSO_4$) and sodium chloride (NaCl) were purchased from Tansoole and used as received. The water used in the present study was ultrapure water (Milli-Q) with a resistivity of 18.2 MΩ cm.

2.2. Synthesis of p(NIPAM-co-VIM) microgels

The thermo-sensitive microgel was prepared via surfactant-free precipitation polymerization using NIPAM as main monomer, VIM as co-monomer and BIS as crosslinking agent. Both microgels of 100 wt% NIPAM (coded PNV0) and of 20 wt% VIM (coded PNV2) were prepared with a crosslinking density of 5 wt% (~3.5 mol%). Typically, the total amount of monomer was kept at 0.8 g and the initiator concentration was fixed at 0.16 mg/mL. A given amount of NIPAM, VIM and BIS were fully dissolved in 100 mL of ultrapure water in a three-necked flask under magnetic stirring at 150 rpm before being heated up to 70 ^{o}C. Simultaneously, oxygen was eliminated by nitrogen bubbling rapidly for 20 min before 10 mL of AIBA aqueous solution was added to initiate the precipitation polymerization. The reaction was kept at 70 ^{o}C for 6 h under protection of nitrogen atmosphere. Once finished, the dispersion was cooled down to 25 ^{o}C

under magnetic stirring and the microgels were fully purified with Milli-Q water via three cycles of centrifugation (7000 rpm for 30 min) before being redispersed in fresh Milli-Q water. Note that a higher VIM feeding ratio (e.g 30 wt%) was also tried while did not result in a very good colloidal stability and hence not recommended.

2.3. Characterizations

Scanning electron microscopy (SEM). One drop of the as-prepared microgel dispersion was deposited onto a clean silicon wafer and dried in air at room temperature before being observed in a scanning electron microscope (Regulus 8100, Japan HITACHI) at an accelerating voltage of 5 kV.

Fourier Transform Infrared (FTIR). FTIR spectra of the microgel samples were collected in a Thermo Nicolet 5700 FTIR Spectrometer with a scanning range of 400 to 4000 cm^{-1} and a minimum of 36 scans (KBr pellets).

Nuclear magnetic resonance (NMR). ^{1}H NMR spectra were recorded on a Bruker ARX 400 spectrometer (400 MHz) at room temperature using D_2O as solvent.

X-ray photoelectron spectroscopy (XPS). XPS spectra were obtained using a ESCALAB Xi+ XPS system (Thermo Fisher Scientific) with a monochromated Al Kα X-ray radiation (1486.6 eV).

Dynamic Light Scattering (DLS). The measurements of hydrodynamic radii (R_h) of microgel particles were conducted in an angle-dependent DLS setup of

an ALV goniometer equipped with a HeNe laser of λ = 633 nm, a digital hardware correlator and two avalanche photodiodes. The temperature of an index match-bath filled with toluene was adjusted using a programmable cryostat (Julabo F32). For each measurement, scattering angles were varied between 30° and 52° in 2° steps with a measurement time of 90 s for each angle. The samples for measurement were highly diluted to minimize multi-scattering. The decay rate Γ from a second-order cumulant fit was plotted against q^2 (q is the magnitude of scattering vector) and a linear regression of the plot was done to determine the diffusion coefficient ($\Gamma = q^2 D_0$)[45]. The hydrodynamic radii were calculated based on the Stokes-Einstein equation as a reference of particle size.

The electrophoretic mobility of the microgel particles were measured using a Zetasizer NanoZS (Malvern Panalytical, USA). Measurements were taken at different temperatures ranging from 25 °C to 70 °C at 5 °C steps after equilibrating the samples at each measurement temperature for at least 5 min. Before all measurements, the samples were filtered with a 1.2 µm cellulose acetate filter.

Static Light Scattering (SLS). The particle form factors of the microgels were obtained via SLS measurements on a closed goniometer (SLS-Systemtechnik GmbH), equipped with lasers of various wavelengths. The temperature of toluene bath as surrounding medium was controlled by a thermostat (Julabo CF40) connected to the goniometer. The samples were highly diluted to

minimize multiple scattering and contributions to the structure factor, and filtered using a 1.2 μm cellulose acetate filter before measurement. Wavelength of λ = 407 nm (covering a *q*-range of 0.007 nm^{-1} to 0.04 nm^{-1}) was used. The scattering intensity was detected at angles varying from 15° and 150° in 1° steps and corrected by subtraction of the solvent scattering. The form factors obtained were fitted by the fuzzy sphere model [46].

2.4. Foam test

To demonstrate the feasibility of developing a responsive flotation for selective Cu^{2+} recovery, it is vital to first evaluate the foamability and foam stability of the as-prepared microgels, especially focusing on its responsiveness to Cu^{2+}. For the foam test of pure PNV microgels, a 2 mL 0.267 wt% microgel dispersion was loaded into a 20 mL quartz tube before being subjected to a vigorous hand shaking for 1 min to generate foams, and the evolutions of foam heights with time and temperature were measured, respectively. For comparison purpose, foam was also generated under identical conditions using sodium dodecyl sulfate (SDS) aqueous solution (0.01 M). To examine potential responsiveness of the foams to Cu^{2+}, foams were prepared with PNV microgels dispersed in $CuSO_4$ solutions with varied concentrations under orbital shaking for 12 hours before being subjected to foam productions. Foam tests of microgel dispersions in other salt solutions of NaCl, $ZnSO_4$ or $MgSO_4$ with varied concentrations were also conducted separately for comparison. Likewise, to evaluate the Cu^{2+}

selectivity, foam tests were conducted under identical conditions in multi-component systems containing 0.005 M Mg^{2+}, Zn^{2+} and Na^{+}, mixed with Cu^{2+} of varied concentrations. Moreover, evolution of foam morphology with time was recorded using snapshot in an optical microscope (Shenzhen Ai Ke Xue, co. Ltd.)

2.5. Interfacial study

Surface tension and dilatation moduli measurement.

The dynamic interfacial tensions between air and microgel dispersions and the corresponding dilatational rheology were measured using a tensiometer of Krüss DSA100 Drop Shape Analyzer (Germany) equipped with a computer-controlled oscillating drop module (DS3270). 10 mL of microgel dispersion (e.g. 0.01 wt%) was loaded in a clean glass chamber with the temperature controlled with an external *Julabo* thermostat. A stainless hook needle (with a capillary tip of 1.493 mm) connected with a 0.5 mL gas-tight syringe (Hamilton co., USA) was immersed in the liquid and, a 10 µL air bubble was created at the tip of the needle with the aid of a micro-syringe pump of DS3270. The bubble shape contour was recorded with time at a constant frame rate (2 fps) and fitted by the Young-Laplace equation to obtain the surface tension. For the measurements of oscillatory dilatational moduli (i.e. storage modulus *E'* and loss modulus *E"*), after generation of an air bubble the surface tension was first allowed to reach a steady value or a meso-equilibrium stage with no oscillation of the interface.

Once the surface tension was equilibrated, the bubble was oscillated at a specified frequency. In principle, an amplitude (i.e. surface area) sweep was performed between 0.1 and 100% at a frequency of 1 Hz to identify linear regime, and then frequency sweeps were performed between 0.1 and 10 Hz at a fixed amplitude (e.g. 5% or 60%). The measurements were done at least in triplicate.

Interfacial shear rheology. The shear rheology of the air−aqueous interface laden with particles was measured using a stress-controlled Discovery Hybrid Rheometer (HR20) (TA Instruments) equipped with a Du Noüy ring (DDR) geometry (platinum ring with diameter ~19.4 mm and wire diameter ~0.4 mm). To achieve maximum measurement sensitivity, the instrument was calibrated using precision mapping with the transducer bearing mode set to soft. A 3.7 mL microgel dispersion (concentration 0.53 wt%) was gently pipetted in the circular Delrin trough to a level that the interface was pinned at the inner edge of the trough, minimizing any effect of the liquid meniscus.

The DDR geometry, rinsed beforehand with ethanol and excess ultrapure water and flamed to remove any organic contaminants, was gently lowered and positioned to pin the air-aqueous interface. A pre-shear (10 s^{-1} for 30 s) was performed to remove any shear history and to guarantee a homogeneity of the interface before a time sweep test (angular frequency ω of 1 rad/s and strain amplitude γ_0 of 0.3 %) was conducted at 25 °C to evaluate the formation of a reliable interfacial film at the air/water interface via the spontaneous adsorption

of the microgel particles. Only when the moduli versus time reached equilibrium (in about 4 hours) indicating the completion of microgel adsorption at air/water interface, other oscillatory measurements were started to be performed. Temperature ramping test (ω 1 rad/s and γ_0 0.5 %) was conducted at temperatures ranging from 25 ^{o}C to 70^{o}C with a ramping rate of 1 ^{o}C/min. More details describing the experimental technique and procedures such as the decoupling of the subphase drag contribution from surface viscosity measurement, etc. can be found elsewhere [47, 48].

2.6. Batch Cu^{2+} sorption

To evaluate the selective Cu^{2+} recovery performance of the as-prepared PNV2 microgel, batch sorption experiments were performed both in pure Cu^{2+} solutions and in mixed Cu^{2+} solutions containing 0.005 M competitive ions (Mg^{2+}, Zn^{2+}, Na^{+}) with varied Cu^{2+} concentrations (i.e. 0.001, 0.0025, 0.005 M). The solid content was fixed at 1 g/L with a total liquid volume of 16 ml as prepared individually in polypropylene centrifuge tubes. After shaking in an orbital shaker (200 rpm) for 24 hours, the sample tube was centrifuged at a speed of 11,000 rpm for 15 minutes, and the supernatant was decanted and filtered with a 0.45 μm syringe filter. Both the Cu^{2+} concentrations in the supernatant and that in the initial solution before sorption were measured by ICP-OES (Optima 8000, Singapore, PerkinElmer).

The amount of Cu^{2+} sorbed by the microgel, q (mg/g), was determined based on following equation:

$$q = \frac{(C_O - C_e)\mathrm{V}}{\mathrm{m}} \qquad (1)$$

where C_o and C_e are the initial and equilibrium concentration (mg/L) of Cu^{2+} in the solution, determined by ICP-OES, V (L) represents the suspension volume and m (g) is the adsorbent mass, respectively.

3. Results and Discussion

3.1 Preparation of thermosensitive poly (N-isopropylacrylamide-co-vinyl imidazole) microgel and effect of Cu^{2+} complexation

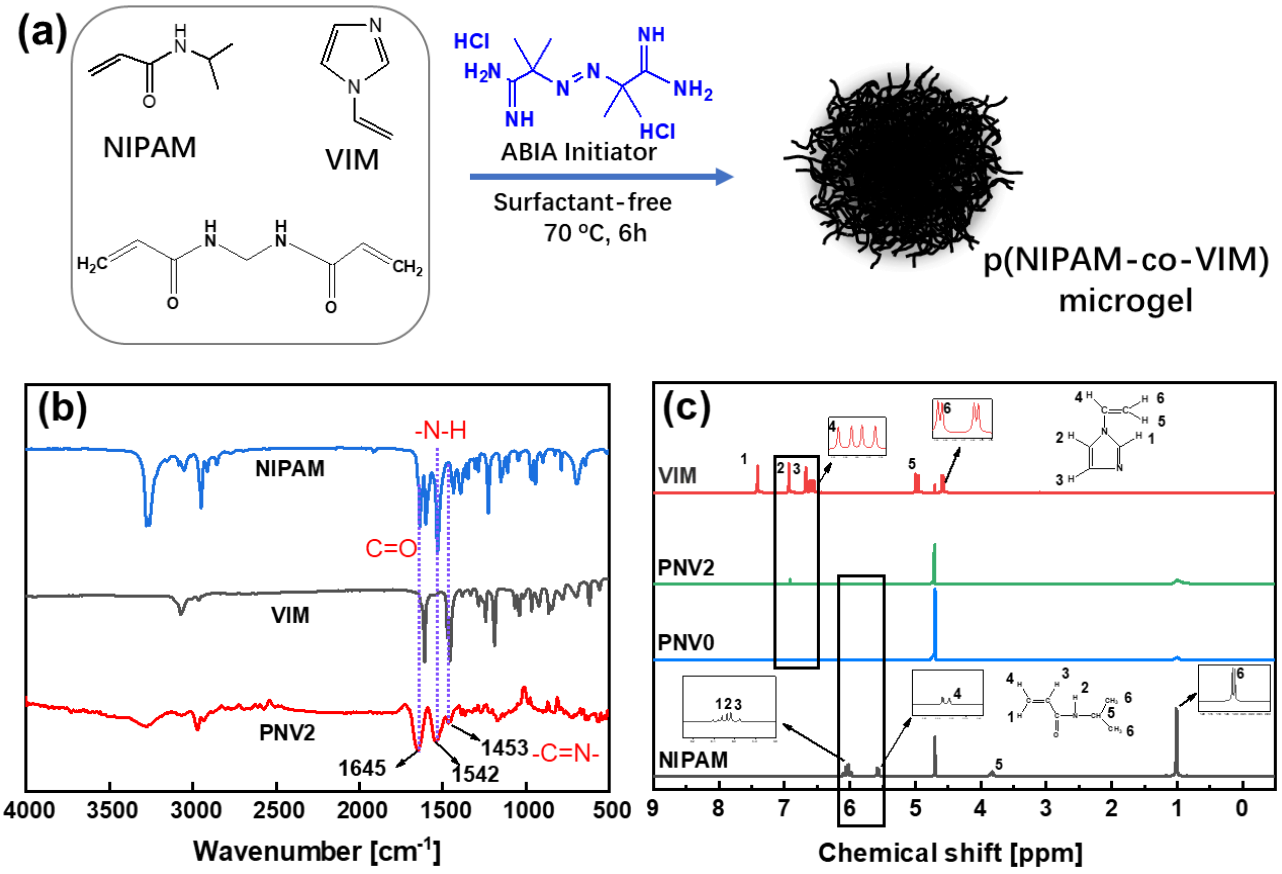

Figure 1. Synthesis of p(NIPAM-co-VIM) microgel (a) and characterizations via FTIR (b) and ^{1}H NMR (c)

As shown in Figure 1a, the thermo-sensitive PNV microgels were synthesized via copolymerization of N-isopropylacrylamide (NIPAM) and 1-vinylimidazole through surfactant-free precipitation polymerization using AIBA as the initiator and BIS as the crosslinking agent. The AIBA, able to disassociate, also acted as cationic stabilizer of the particles, ensuring the dispersion to be stable during the polymerization. FTIR and ^{1}H NMR analysis were used to confirm the synthesis of the PNV microgels, with results shown in Figure 1b and 1c, respectively. In the FTIR spectra, the characteristic peaks of $\nu_{C=O}$ and ν_{N-H} at 1645 and 1542 cm^{-1} were observed in both p(NIPAM-co-VIM) and NIPAM, and the characteristic peak of $\nu_{C=N}$ at 1453 cm^{-1} were observed in both p(NIPAM-co-VIM) and VIM. This indicates the existence of NIPAM and VIM in the p(NIPAM-co-VIM) microgels. In the ^{1}H NMR spectra (Figure 1c), the data of PNV2 and PNV0 are shown in comparison to that of NIPAM and VIM monomers. The strong peak at 4.7 ppm was the peak of D_2O solvent. The signals of the unsaturated carbon bonds in the monomers (i.e. proton 1,3,4 in the chemical structure of NIPAM and proton 4,5,6 in that of VIM) disappeared in the spectra of both PNV2 and PNV0, indicating a full conversion of the monomers during the polymerization process. The signals at 6.5-7.5 ppm clearly observed in the VIM monomer are attributed to the imidazole group (proton1,2,3 in the chemical structure of VIM), and remained observable in the spectrum of PNV2 around 6.9 ppm, while undetectable in PNV0. Note that the weaker signals in the PNV2

and PNV0 can be somewhat due to the fact that the microgel particles were more swelled but less dissolved in solvent, consistent with the literature[49]. Anyhow, the characteristic peaks observed in the NMR spectra are able to confirm the presence of both the NIPAM and VIM units in PNV2 while NIPAM unit only in PNV0. This, together with the FTIR analysis, demonstrates the successful synthesis of the p(NIPAM-co-VIM) polymers.

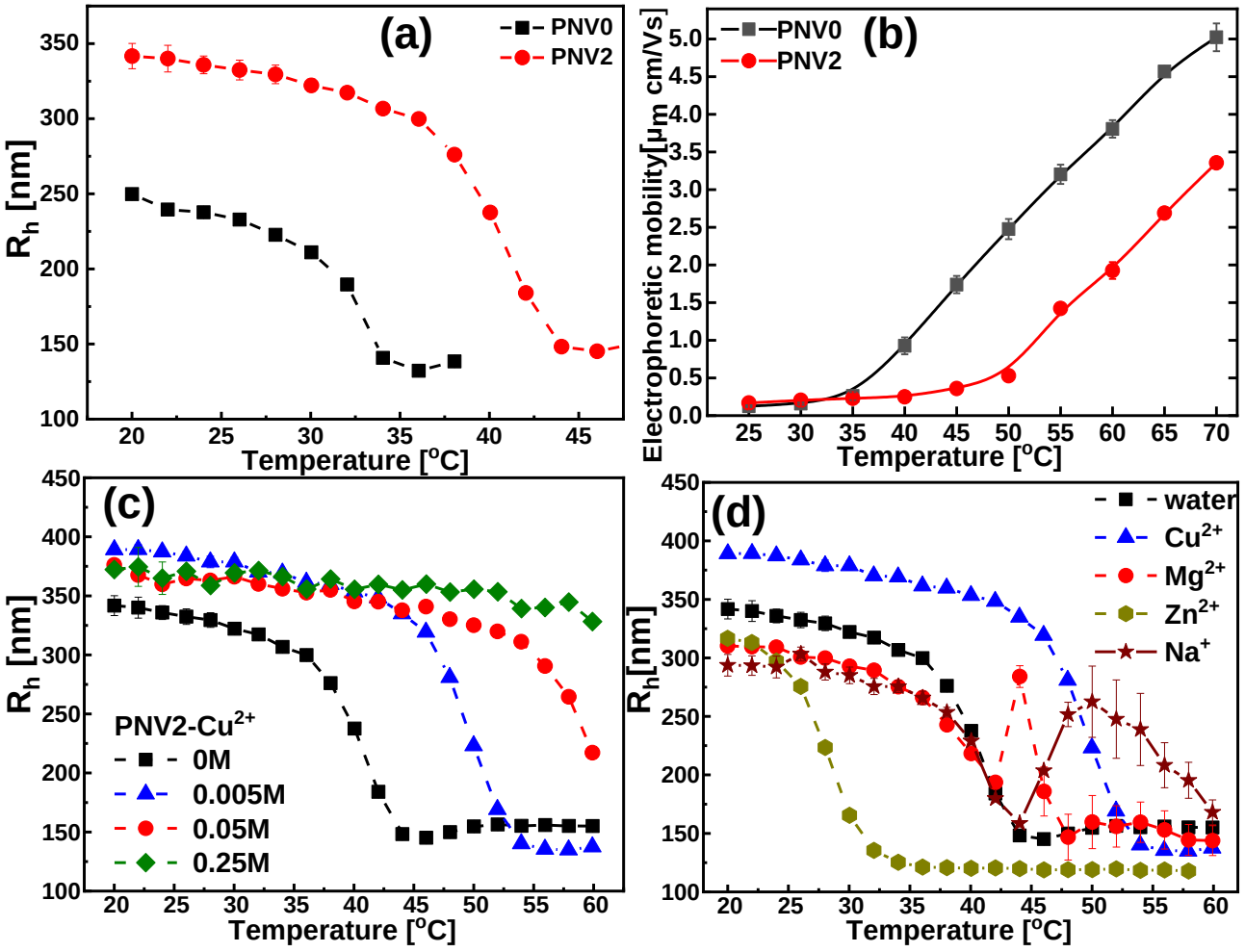

Figure 2. Hydrodynamic radii R_h (a) and electrophoretic mobility (b) of PNV0 and PNV2 as a function of temperature; temperature dependence of R_h of PNV2 in the presence of Cu^{2+} with varied concentrations (c), and in the presence of different cations (0.005 M) (d)

Furthermore, SEM image in Figure S1 in the Supplementary Material confirms the monodisperse spherical morphology of the microgel particle with a narrow particle size distribution, having an average diameter estimated to be 455 ± 35 nm for PNV2. The DLS measurements of hydrodynamic radii R_h as a function of temperature (see Fig.2a) show the clear temperature responsiveness of the PNV microgels: a large R_h value below VPTT when the microgels were in swollen state while the R_h underwent a rapid decrement to the smallest value above the VPTT when the microgels were in shrunk state. Obviously, the incorporation of VIM comonomer shifted the VPTT of pNIPAM (i.e. PNV0) from ~32.5 ^{o}C to ~40 ^{o}C and the swelling ratio (R_h at 20^{o}C to the smallest R_h) was increased from1.89 ± 0.10 for PNV0 to 2.35 ± 0.10 for PNV2. This is consistent with findings reported in some earlier studies[49-51], and was considered plausible as the presence of VIM segments could hinder the collapse of the PNIPAM chains and induce a higher swelling, in light of its hydrophilic character and electrostatic repulsion between partially ionized VIM groups[52]. Note that the size measured by the DLS is basically in accordance with that of SEM characterization (Fig.S1), considering the difference in technique.

Figure 2b shows the electrophoretic mobility (zeta potential) of the microgel particles as a function of temperature. As can be seen, at the temperature of

polymerization(70 ^{o}C), the particles were well positively charged with a relatively high electrophoretic mobility (i.e. ~5.0 μm cm/Vs for PNV0 and ~3.5 μm cm/Vs for PNV2). This is a result of the decomposition of cationic initiator AIBA into positively charged amidino groups locating at the peripheries of particles. Such presence of surface positive charges guaranteed a good colloidal stability during the surfactant-free polymerization. As the temperature decreased, the particle surface charge density was observed to gradually decrease towards a constant close to 0 μm cm/Vs especially when the temperature was below the VPTT. This was a result of particle swelling and is consistent with the literature [53]. The smaller electrophoretic mobility of PNV2 than PNV0 must be associated with its higher VPTT and larger swelling ratio with reduced surface charge density.

As is known, regardless of the low surface charge density, the colloidal stability below VPTT was believed to be good thanks to the fuzzy sphere structure of the swollen microgel as a result of inhomogeneous crosslinking. The dangling chains from the loose crosslinked shell of the swollen microgel could barrier the microgels from aggregation via steric repulsion [54]. Note that the particles might be more susceptible to partial aggregation if being long-time heated in a temperature range above but close to the VPTT when the particle surface charge keeps low.

Figure 2c shows the effect of Cu^{2+} on the temperature dependence of R_h of PNV2 microgel. Evidently, the presence of Cu^{2+} enhanced the swelling behavior

of PNV2 microgel and greatly affected its thermo-sensitivity by shifting the VPTT from ~40 °C to ~50 °C for 0.005 M Cu^{2+}, to ~60 °C for 0.05 M Cu^{2+}, and to a value out of measurement temperature range for 0.25 M Cu^{2+}, respectively. This was attributed to the effect of ion complexation between Cu^{2+} and imidazole groups in VIM segments within PNV2 microgel. The Cu^{2+}-imidazole complexation was confirmed by XPS measurement (see Figure S2). Both the appearance of an additional peak around 401.54 eV in the deconvoluted N 1s peaks of PNV2-Cu sample, and the appearance of 933.43 eV in the deconvoluted Cu 2p peaks are considered to be the contribution signals of the Cu^{2+}-imidazole complexation [55, 56]. The broad concentration range focused here is to resemble contamination scenarios obtainable in practical effluents and also to better show the trend of Cu^{2+}-ligand complexation effect on microgel behavior.

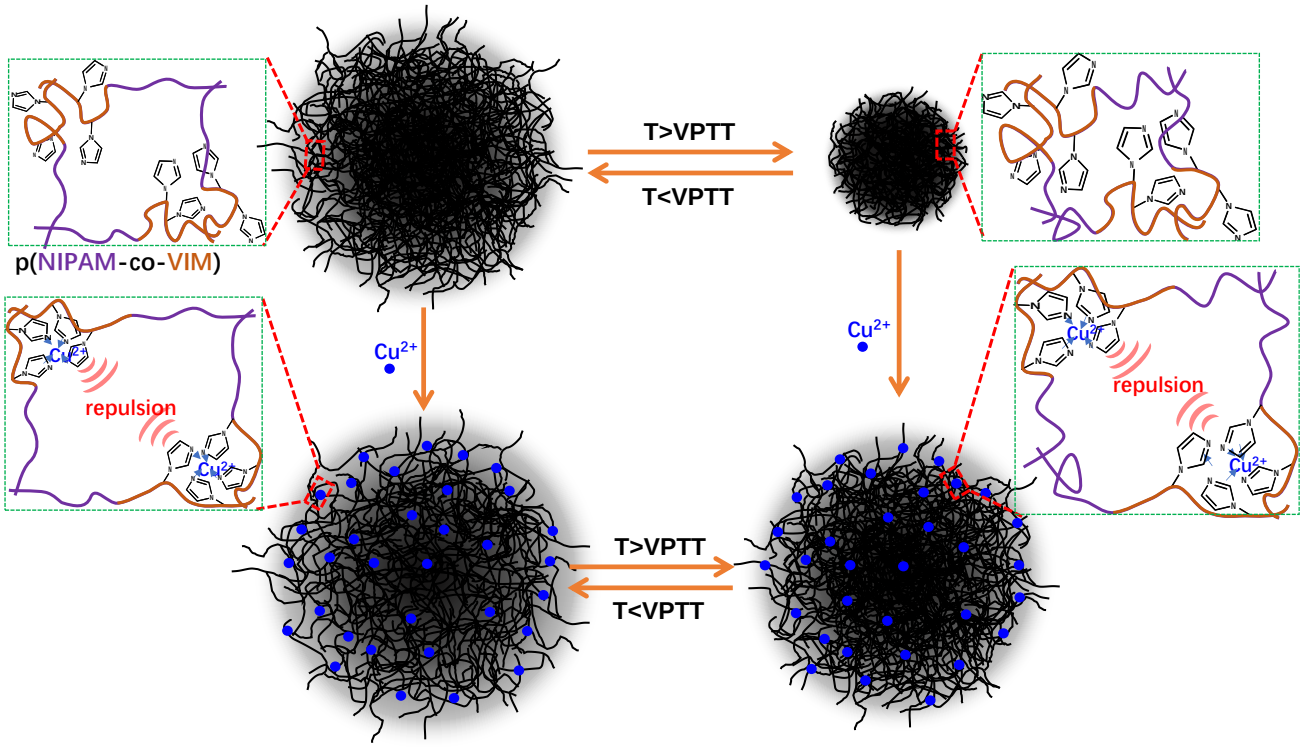

Scheme 1. Effect of Cu^{2+} complexation on swelling property of PNV microgel

As shown in Scheme 1, for a typical pNIPAM-based microgel, the swelling happened along with stretching of pNIPAM chains as induced by the formation of hydrogen bonds between water and amide groups and the deswelling was accompanied with shrinking of the pNIPAM chains when the hydrogen bonds were removed above the VPTT. In PNV2, Cu^{2+}-imidazole complexations were likely to induce electrostatic repulsions between the VIM segments within particles. This, together with increased hydrophilicity via ion solvation of Cu^{2+}, further enhanced the swelling degree of the swollen PNV2 microgel. This can also be partly aided by the osmotic pressure difference in and out of the particle caused by the Gibbs-Donnan effect. When heating above the VPTT, the strong interactions between Cu^{2+}-complexed VIM segments can significantly balance the hydrophobic interactions between pNIPAM chains and hence resist the network shrinkage of the p(NIPAM-co-VIM). This was well manifested by the great shift of the VPTT to higher temperatures (Fig.2c). Moreover, the Cu^{2+}-imidazole complexation guaranteed a very good colloidal stability and good swelling/deswelling reversibility of the PNV2 microgels, as confirmed by the curve overlapping of temperature dependence of R_h upon repeatedly heating and cooling (see Figure S3).

Note that there can have various types of competitive ions coexisting with Cu^{2+} in wastewater [57], instead of covering all the possible ions, this study only

selected a limited number of representative cations from different metal family groups for a purpose of comparison with Cu^{2+} to test the responsive characteristics of the microgel. The selected cations included bivalent transitional metal ion Zn^{2+}, alkaline earth metal ion Mg^{2+}, and well-known alkali metal ion Na^{+} that often exist in aqueous environment as competitive ions of Cu^{2+}. The selected ions were reported to have a much weaker complexation affinity (Zn^{2+}, with an overall stability constant *log K* ~ 4.8 comparing to *log K* ~ 48.4 of Cu^{2+}) [44], or no complexation (Mg^{2+}, Na^{+}) to imidazole than Cu^{2+}. Indeed, Zn(II) was demonstrated to prefer oxygen donors over nitrogen ones [44]. Similarly, some other commonly coexisting cations such as Fe^{2+}/Fe^{3+} and Al^{3+} also show more affinity to oxygen-based ligands such as catechol groups[58, 59] rather than to imidazole group. As shown in Figure 2d, different from Cu^{2+}, all the selected cations lightly decreased the hydrodynamic diameter at temperatures below the VPTT. Such “salt-out” effect of de-swelling the particles as a result of dehydration of the pNIPAM chains by electrolyte was consistent with earlier studies[60]. Both Na^{+} and Mg^{2+} exhibited no much effect on shifting the VPTT of the microgel, nevertheless, induced partial aggregations of particles when temperature across the VPTT due to the particle surface charge screening effect. Such destroy of colloidal stability became even more pronounced with increased electrolyte concentration (see Fig.S4). For Zn^{2+}, a negative shift of VPTT was observed, which was most likely due to the preferred complexation of Zn^{2+} to oxygens in amide groups of pNIPAM chains that greatly destroyed

their hydrogen bonding with water. Likewise, higher concentrations induced particle aggregations (Fig.S4b). Undoubtedly, such differences between the cations enable an easy discrimination and provide guide for detection and selective recovery of Cu^{2+} from competitive ions.

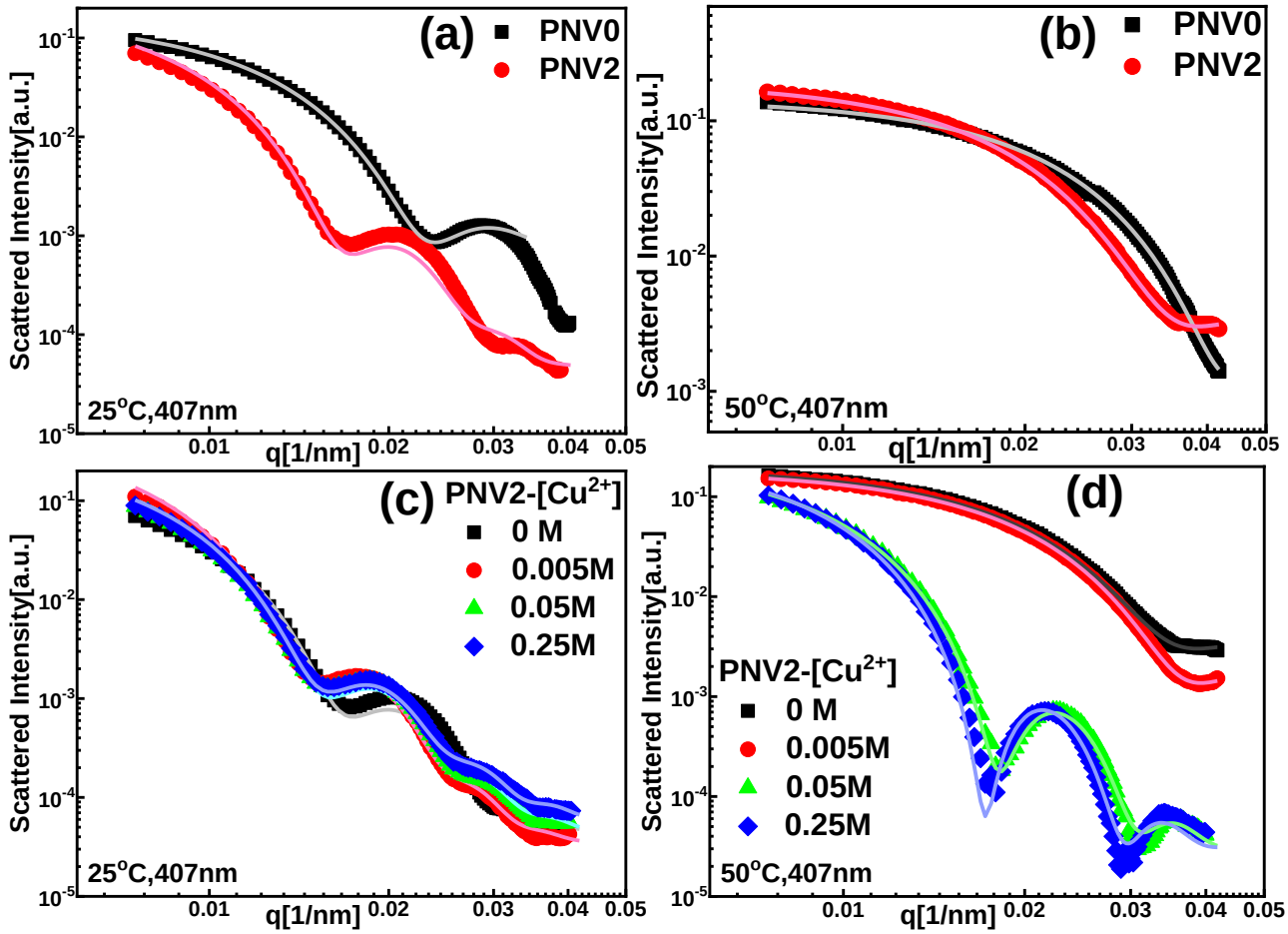

Figure 3. Particle form factors probed via SLS of PNV microgels (a-b) and Cu^{2+} complexed PNV2 microgels (c-d) at 25 °C (a,c) and 50 °C (b,d). Solid lines represent the fittings of the fuzzy sphere model.

Moreover, the internal structure of PNV0 and PNV2 microgels without and with Cu^{2+} complexations at 25 °C and 50 °C was investigated in terms of particle

form factor analysis as probed by static light scattering (SLS). Fig.3 presents the SLS data of the microgels and the fuzzy sphere model by Stieger et al [46] was used to fit the data. The model describes the radial scattering length density by a box function convoluted with a Gaussian to account for the surface fuzziness of the microgels. The form factor, $P_{inho}(q)$, was described as follow:

$$P_{inho}(q) = \left[\frac{3[\sin(qR)-qR\cos(qR)]}{(qR)^3}\exp\left(-\frac{(\sigma_{surf}q)^2}{2}\right)\right]^2 \quad (2)$$

where q is the scattering vector, R is the fitting radius of the microgel, and σ_{surf} accounts for the width of the surface fuzziness. The overall size obtained by SLS was approximately given by $R_{sls} = R + 2\sigma_{surf}$.

At 25 °C, the model fit can basically match the experimental data of PNV0 and PNV2 over a broad q-range, resulting in a radius of R_{sls} = 195 ± 7.3 nm and a width of fuzzy periphery of σ_{surf}= 30 nm for PNV0, and R_{sls} = 331 ± 10 nm and σ_{surf}= 37.2 ± 7.9 nm for PNV2. For the PNV2 microgels complexed with Cu^{2+} (0.005M, 0.05M and 0.25M), the scattering peak was shifted to a lower q value and the data of particle form factor can be well described by the fuzzy sphere model, indicating a perfect spherical shape even in the swollen state. The physical parameters extracted from the fittings are listed in Table 1. In general, after complexation the microgels exhibited a higher R_{sls} value while a similar fuzziness as compared to the pure PNV2, implying that the Cu^{2+} complexation better swelled and homogenized the polymer networks.

At 50 °C, the particle form factor data of all the microgels without and with

Cu^{2+} complexation are very well fitted by the fuzzy sphere model, indicating a very good sphere shape of the particles. For PNV0 and PNV2, the microgels were in its collapsed state, having R_{sls} = 123 ± 4.4 nm and σ_{surf} = 10.7 ± 5 nm for PNV0, and R_{sls} = 148 ± 8 nm and σ_{surf} = 5.1 ± 10 nm for PNV2. The fitting data (see Table1) of the complexed microgels confirmed that the PNV2 complexed with 0.005 M Cu^{2+} was partially de-swollen at 50 °C (R_{sls} = 169 ± 9.5 nm and σ_{surf} = 27.2 ± 18 nm) and that of PNV2-Cu^{2+}(0.05 M) and PNV2-Cu^{2+}(0.25 M) were fully swollen. These results are consistent with the DLS measurement. By comparing the scattering data between the microgels, it is not difficult to conclude that VIM enhanced the swelling behavior of the microgel and Cu^{2+} complexation further swelled and softened the microgels, with the microstructure and softness tunable by Cu^{2+} concentration.

Table 1 Radii and form factor parameters of PNV microgels

Sample	25°C			50°C		
	R_h (nm)	R_{sls} (nm)	σ_{surf} (nm)	R_h (nm)	R_{sls} (nm)	σ_{surf} (nm)
PNV0	235.5±1.7	195±7.3	30±2.9	132±0.8	123±4.4	10.7±5
PNV2	334±2.2	331±10	37.2±7.9	157.8±0.5	148±8	5.1±10
PNV2-Cu^{2+} 0.005M	384±2.3	380±9	46±2.8	223±1.5	169±9.5	27.2±18
PNV2-Cu^{2+} 0.05M	364±3.3	350±10	35±8.8	325±2.2	297±3.7	22.2±8.5
PNV2-Cu^{2+} 0.25M	369±2.2	343±11	31.8±10	356±0.5	355±2.8	47.7±2.9

Aside from the microstructure of single microgel studied here by light scatterings, it is worthwhile mentioning that the colloidal phase behavior and collective interactions of microgels in bulk suspension, which can be accessed via rheology [61] or gel point determination [62], etc., can also be of significance for its application, notwithstanding it is beyond the main focus of this study.

3.2. Foamability and foam stability

The as-prepared thermo-sensitive PNV microgel dispersions were used to produce Pickering foams by hand-shaking. The initial foam height and its evolution with time were used to evaluate the foamability of the microgels and the foam stability. As shown in Figure 4a, an initial foam height ~25 mm for PNV0 and ~30 mm for PNV2 indicates an excellent foamability of the as-prepared microgel dispersions.

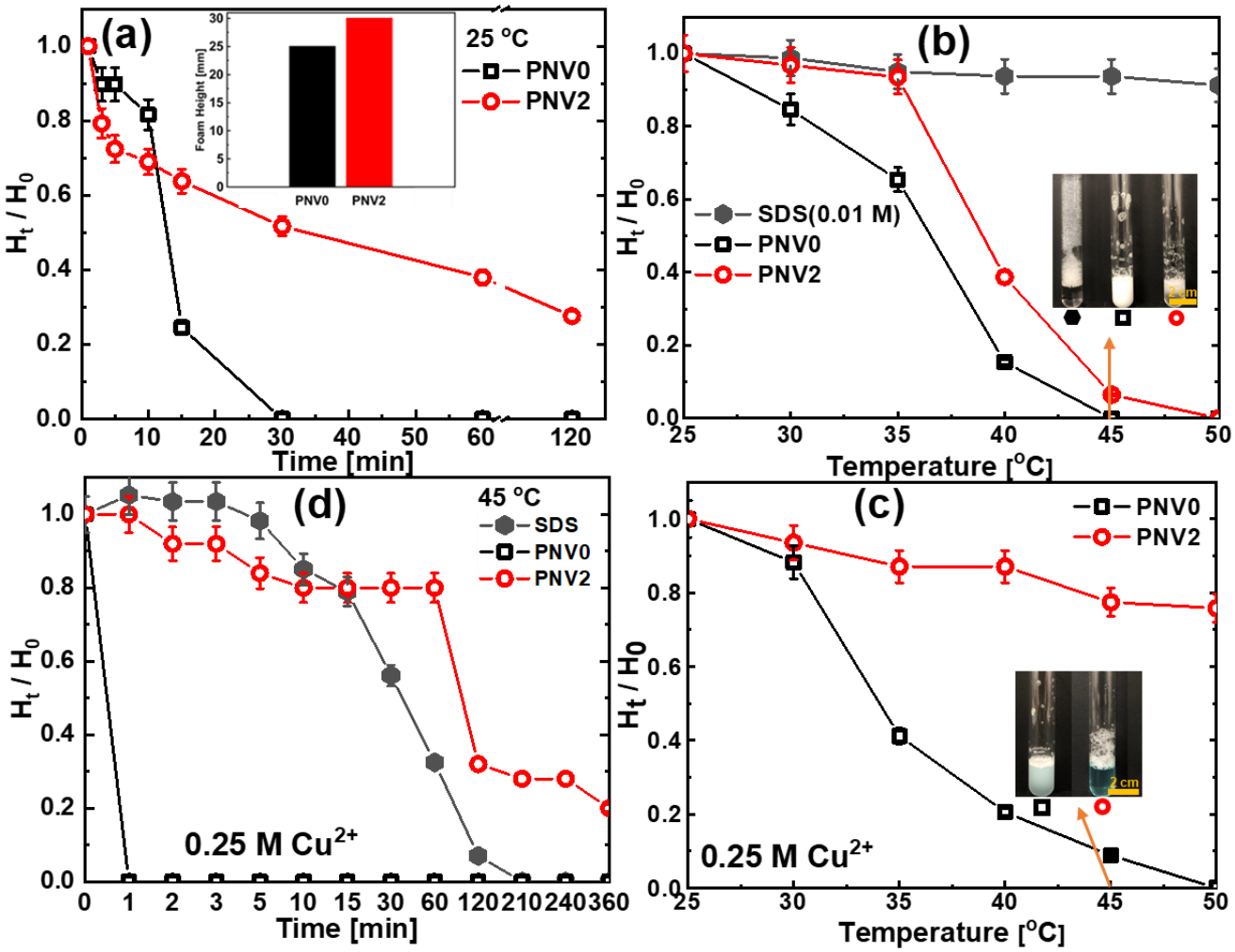

Figure 4. Foam height plotted in term of height at time *t* versus initial height (H_t/H_0) as a function of time (a: 25 °C, d: 45 °C) and of temperature (b,c) for PNV0 and PNV2 microgels in the absence (a-b) and in the presence of Cu^{2+} (0.25M) (c-d). Foams produced from 0.01 M SDS solution was used as reference. Inset in (a) the initial foam height and insets in (b, c) photos of foams after being heated to 45 °C.

It is clear that there are differences on foam stability between PNV0 and PNV2 microgels. After a rapid reduction within the first 5 minutes that must be associated with liquid drainage, and a short-period (c.a. 5 mins) of slow decay,

the foam height in PNV0 experienced an abrupt descent to 0 mm within 30 min indicating a rapid foam collapse that might be due to bubble coalescence. However, for PNV2, after a similar rapid reduction within the first 5 minutes, the foam height attenuated with a steady and slower rate, a long-term destabilization trend mostly reported as a result of bubble coarsening. This indicated an enhancement of VIM on the foam stability of the pNIPAM-based microgels.

Fig. 4b shows the effect of temperature on foam height of the PNV microgel dispersions, using the foams generated from 0.01M SDS solution as reference. The whole heating experiment from 25 °C to 50 °C took about 10 minutes, a time length that the foams remained stable at 25 °C (Fig.4a). As shown in Figure 4b, the foams stabilized by PNV microgels experienced an abrupt reduction in foam height towards zero above a critical temperature roughly around their VPTT. This was in great contrast to the foams stabilized by SDS, which maintained its good stability at high temperatures with a very slight reduction in foam height. The photos in Figure4b inset showed the difference in foam appearance at 45 °C between SDS and PNV microgels. Undoubtedly, the “smart” feature of thermo-responsive foams stabilized by the as-prepared PNV microgels was thus demonstrated.

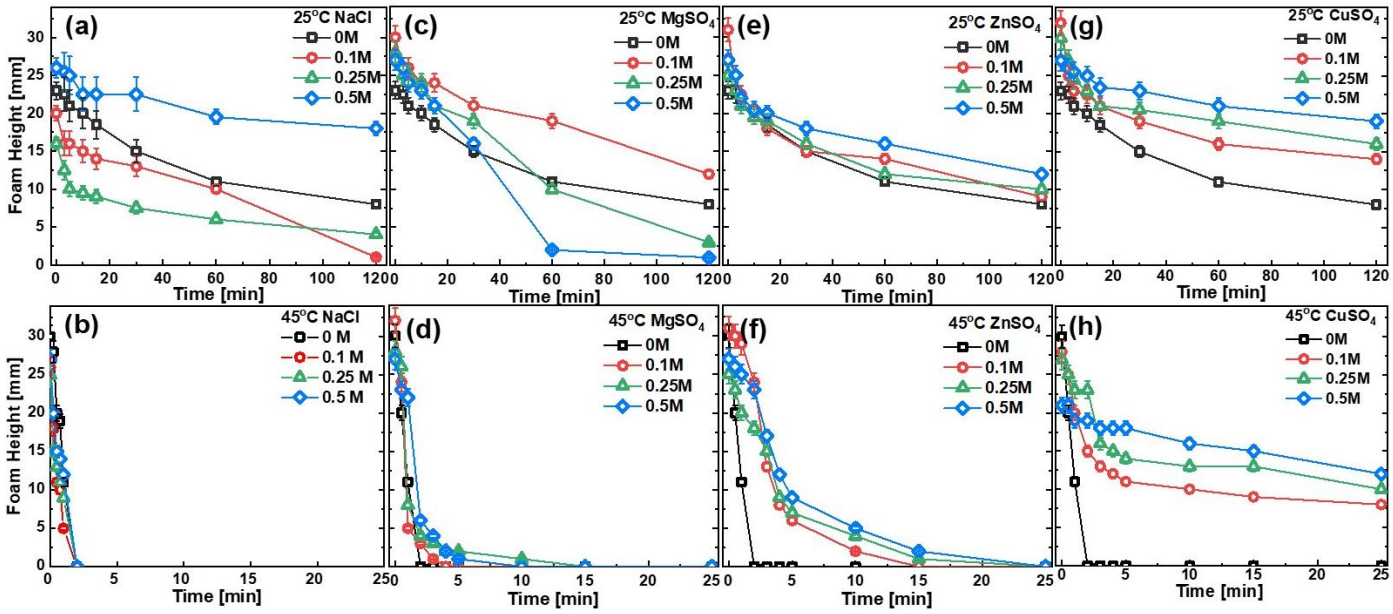

Figure 5. Foam height as a function of time at 25 °C (a,c,e,g) and 45 °C (b,d,f,h) for PNV2 microgels in the presence of NaCl (a-b), $MgSO_4$ (c-d), $ZnSO_4$ (e-f) and $CuSO_4$ (g-h) with varied concentrations (0-0.5 M)

For a typical Pickering foam stabilized by surface-charged solid particles, the addition of electrolyte was believed to have a marked effect on foam stability by altering particle state from well-dispersed to aggregated and thus affecting bubble coalescence[63]. As shown in Figure 5, at 25 °C, for PNV2 microgels, the electrolytes also show effects on foam stability, with the stability maximized at a specific concentration for a given salt (e.g. 0.1 M for Mg^{2+} and 0.5 M for Na^{+}, Zn^{2+}, Cu^{2+}), with foams maintained stable for at least 120 min. Different from other cations, the Cu^{2+} shows a very clear linear increase on foam height with increased Cu^{2+} concentration.

At 45 °C (a temperature above the VPTT of PNV2 microgel), the foams became fully collapsed rapidly after preparation, within ~ 2 min, ~10 min and

~15 min for Na^+, for Mg^{2+} and Zn^{2+} solutions, respectively, showing almost independence of salt concentration (Fig.5b,d,f). Nevertheless, for Cu^{2+}, the foams were substantially stable with only a small reduction on foam height when compared to 25 °C, a result of heating-induced liquid drainage at plateau border of foams.

Likewise, from temperature dependence of foam height (Fig. 4c and Fig.S5), the effect of Cu^{2+}-imidazole complexation on foam stability was also clearly demonstrated. In 0.25M Cu^{2+} solution, the foams of PNV0 well kept its good temperature responsiveness with foam height abruptly reduced to zero above the VPTT whilst the PNV2 showed a very subtle temperature dependence of foam height, with Cu^{2+} heavily removed the thermo-sensitivity of the foams. For clarity, the temperature dependence of foam height was evaluated in other salt solutions (i.e. Na^+, Mg^{2+}, Zn^{2+}), with data shown in Figure S5. It was clear that the foams stabilized by either PNV2 or PNV0 microgels exhibited striking thermo-responsiveness with an abrupt collapse above the VPTT in all the selected salt solutions except for Cu^{2+} solution where the foam of PNV2 maintained stable throughout the measured temperature range. Moreover, as shown in Figure 4d, at 45 °C, in the presence of 0.25 M Cu^{2+}, the foam life of PNV2 can be as long as 6 hours, much longer than SDS stabilized foams that collapsed in 2 hours, let alone the foams of PNV0 that rapidly collapsed within 1 minute.

The findings indicate that the responsiveness of “smart” foams stabilized by

thermosensitive PNV2 microgels are tunable by Cu^{2+}, more exactly, via the Cu^{2+}-imidazole complexation that induces particle swelling at a broad temperature range.

The Cu^{2+} responsive microgels can not only be used as a sensor material to detect Cu^{2+} and/or to discriminate Cu^{2+} from competitive ions, but also enable a possibility to develop responsive froth flotation process to selectively recover Cu^{2+} from aqueous environments with competitive ions, especially at high temperatures where the adsorption kinetics of Cu^{2+} was often reported to be enhanced [64]. The as-prepared PNV2 microgels can potentially act not only as adsorbent to uptake Cu^{2+} but also as responsive stabilizer of a froth flotation to spontaneously recover the microgel-based adsorbent from aqueous environment after the Cu^{2+} adsorption. Moreover, apart from its “smart” function, the environment friendly raw materials, the surfactant-free preparation approach and the non-toxic feature of the resultant microgel, can make the flotation to be a very green technology, being greatly contrary to classical flotation that involves the use of hazardous organics.

3.3. Interfacial study of microgels at air-water interface to understand the responsive foaming performance

Undoubtedly, the responsive foam stabilization and destabilization, irrespective of modulation by temperature or by Cu^{2+}, are associated to the swelling and deswelling of the microgel, but the underlying mechanism remains

unclear. To understand how the swelling and deswelling of microgels affects the transitioning of foam stability, here the interfacial behavior of PNV microgels at air/water interface was investigated based on dynamic surface tension and interfacial rheology measurements. It was demonstrated that the Cu^{2+}-complexed PNV2 microgel can be kept in a swollen state and the foam was ultra-stable at high temperatures (e.g. 45 ^{o}C) where the pure PNV2 de-swelled and its stabilized foams collapsed. This makes the PNV2 and PNV2- Cu^{2+} being a good model system to elucidate the underlying mechanism how the microgel deswelling is linked to the foam destabilization in a fixed temperature.

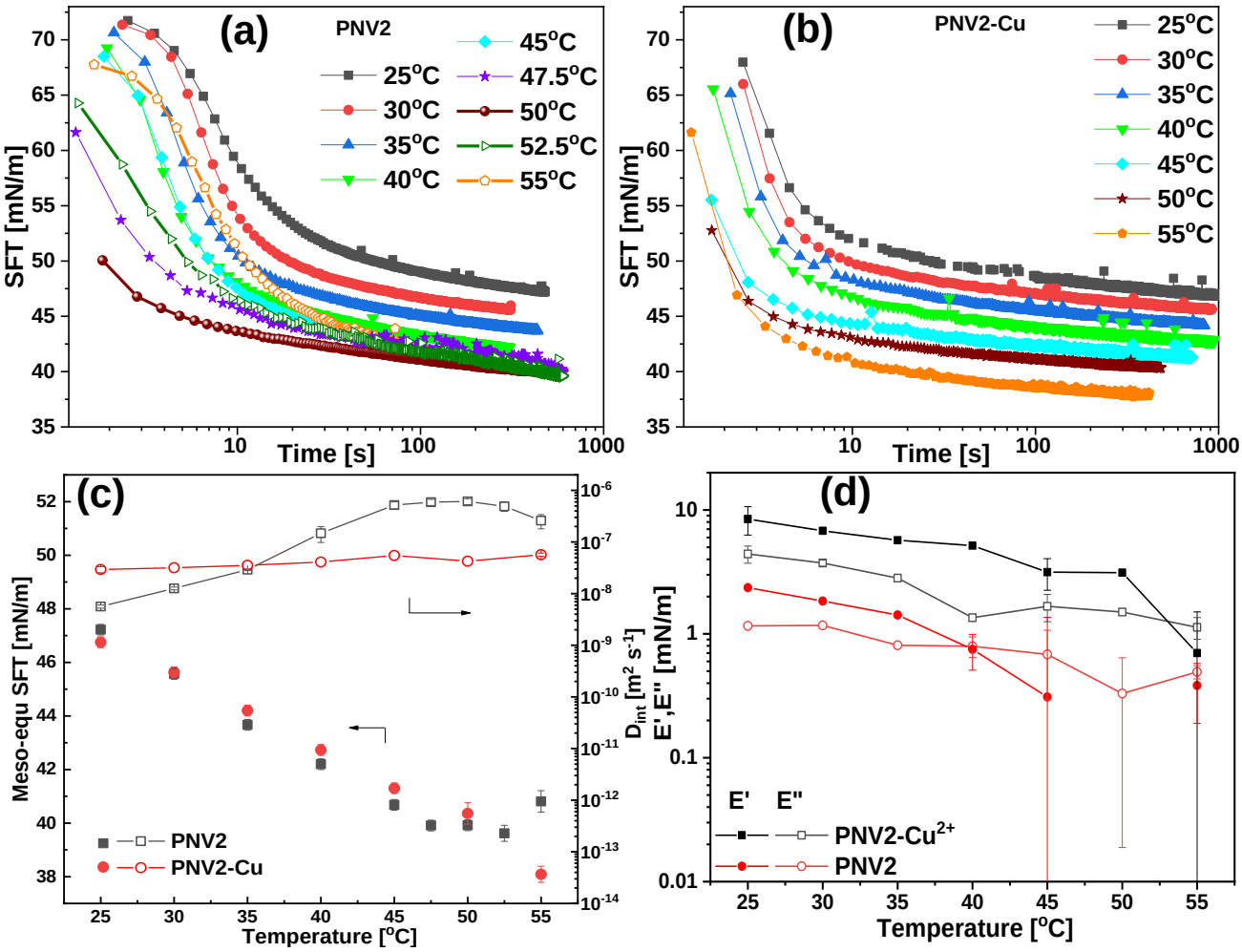

Figure 6. Temperature dependence of the dynamic surface tension (SFT) of air-aqueous dispersions (0.01 wt%) of PNV2 microgel (a) and PNV2-Cu^{2+}(0.25M)(b); Temperature dependence of the corresponding meso-equilibrium surface tension (Meso-equ SFT) and particle diffusivity approaching the interface (D_{int}) (c), and the dilatation moduli (E', E") of PNV2 microgel and PNV2-Cu^{2+} at air-water interface.

Typically, the foamability of a particle has been demonstrated to be related with its ability to partition from solvent and reside at the air–water interface. The adsorption of particles at air-water interface has been extensively manifested to

reduce the surface energy and hence the surface tension, and therefore the change of surface tension can be used to reveal the adsorption dynamics and kinetics at the interface. Figure 6a and 6b show the evolution of air-water surface tension ($\gamma_{a/w}$) with time of PNV2 microgel dispersions (0.01 wt%) at different temperatures without and with Cu^{2+} (0.25 M) (denoted as PNV2-Cu), respectively. Obviously, in both PNV2 and PNV2-Cu, the $\gamma_{a/w}$ underwent a rapid decrease with time at the beginning before transitioning to a sluggish decay period and reached a meso-equilibrium stage. This indicates a spontaneous adsorption of the PNV microgels to the air-water interface with the adsorption rate slowing down with time when the interface was increasingly covered by particles, being greatly consistent with earlier studies[65]. Note that the $\gamma_{a/w}$ decrement happened to all the measured temperatures, irrespective of the presence or not of Cu^{2+}, indicating that both the swollen microgels below the VPTT and the collapsed ones above the VPTT have similar interfacial activity to spontaneously adsorb to the air-water interface.

With regard to the effect of temperature, it can be seen that there are differences on the rate of $\gamma_{a/w}$ decrement at early stage and on the values of meso-equilibrium SFT in late stage. In particular, for the $\gamma_{a/w}$ decrement rate, PNV2 witnessed an increase with temperature till 50 ^{o}C before bouncing back while PNV2-Cu saw only a linear increase with temperature. In fact, before being dominated by the barriers from the adsorbed particles at the interface, the particle adsorption at the early stage to particle-free interface was considered

to be dominated by the diffusivity of particles approaching the interface. The interfacial diffusivity (D_{int}) of PNV2 was determined to be 5.64×10^{-9} m^2s^{-1} at 25 ^oC (Figure 6c), and increased to a maximum of 6.12×10^{-7} m^2s^{-1} around the VPTT, (i.e. 50 ^oC here, considering the difference between the measured temperature in liquid bulk and that at bubble surface), before being decreased with temperature thereafter. Details on the determination of D_{int} and further discussions are given in the Supplementary Material. In contrast, the D_{int} of PNV2-Cu was greater (i.e. 2.94×10^{-8} m^2s^{-1}) than that of PNV2 at 25 ^oC, and less dependent on temperature, having 5.69×10^{-8} m^2s^{-1} at 55 ^oC. This indicates that the great diffusion-limited adsorption of Cu^{2+}-induced swollen particles (i.e. PNV2-Cu) to the air-water interface show a less thermo-sensitivity, providing good particle partitions to the interface with a guaranteed excellent foamability over a broad temperature range.

Moreover, there are differences between PNV2 and PNV2-Cu on the temperature dependence of the meso-equilibrium surface tension (MSFT) (Fig. 6c). Both experienced a linear reduction of MSFT with temperature while the PNV2 reached a plateau ~ 40 mN/m above the VPTT but the PNV2-Cu continued the reduction to ~38 mN/m at 55 ^oC. As having been widely reported[66], microgel exhibits a different interfacial behavior from rigid sphere particles, being able to deform at the water-air (oil) interface with the microgel spreading out like a fried egg at the interface. Such deformation and spreading at the interface contributed to the linear MSFT reduction with temperature below

VPTT. Over the VPTT, the shrunk and rigid particles can fully cover the interface with a saturated and compact state, reaching a plateau in MSFT with no further reduction with temperature (PNV2). For PNV2-Cu, within the measured temperature range (<55 ^{o}C), the particles remained swollen and the change of MSFT with temperature was dominated by the microgel deformation/spreading at the interface, and a further increased particle coverage at the interface was still allowed even above 55 ^{o}C. This definitely confirmed a better surface activity of the softer PNV2-Cu microgels.

The good foamability of PNV microgels (i.e. PNV2 and PNV2-Cu) demonstrated by their superior surface activity, aided by the enhanced interfacial diffusivity with temperature and Cu^{2+}-induced softening, was consistent with the foam data (Fig. 4-5). However, this is still difficult to elucidate the mechanism of responsive destabilization of the PNV microgel-stabilized foams since the microgels in both swollen and collapsed states exhibited good surface activity, excluding the desorption of particles from interface as the reason of responsive foam destabilization.

As to the long-term foam stability, except from liquid drainage, the destabilization mechanisms of bubble coalescence and coarsening (i.e. Ostwald ripening) have been demonstrated to be associated with the mechanical properties of the interfacial films formed by the adsorbed particles[67]]. In general, it was recognized that the bubble coalescence is closely peritent to the shear rheology of the interfacial films while the coarsening

is more dominated by the dilatational rheology[68]. To probe the dilatational viscoelasticity of the interfacial layer, the microgels-laden bubble was subjected to a sinusoidal oscilation on the surface area (*A*) with the corresponding change of surface tension (γ) measured. The dilatational modulus *E* given as : $E = \partial\gamma/\partial LnA$, can be decoupled to an in- phase (elastic) contribution, E', and an out-of-phase (viscous) contribution, E"[69], data of which obtained at 1Hz are ploted in Figure 6d and examples of frequency sweep test shown in Figure S7. As is shown, both the PNV2 and PNV2-Cu were dominated by elasticity (i.e. E'>E") at low temperatures with PNV2-Cu having higher values than PNV2. The moduli were found to decrease with temperature and the PNV2 experienced an abrupt drop in moduli around the VPTT to a liquid-like region (i.e. E">E', surface viscoelasticity dominated by E") whereas the PNV2-Cu maitained its elasticity dominance till 55 ºC. Such difference on dilatational viscoelasticity between PNV2 and PNV2-Cu is consistent with their foam stability that the PNV2 exhibited a thermo-responsiveness having foam collaption across the VPTT, in great contrast to the ultra-stability of PNV2-Cu at high temperatures. Note that, there was a Gibbs criterion reported for emulsion stability against coarsening by Ostwald ripening, that is, a dilatation modulus E >γ/2 is unfavorable for Ostward ripening[17, 69]. Unfortunately, the *E* values of both the PNV2 and PNV2-Cu are less than 10 mN/m while their γ/2 values are ~ 20 or ~19 mN/m, not satisfying the Gibbs criterion. That means even though the PNV2-Cu has a higher dilatational elasticity than PNV2, but the destabilizaiton mechanism of

coarsening seems not be well hampered.

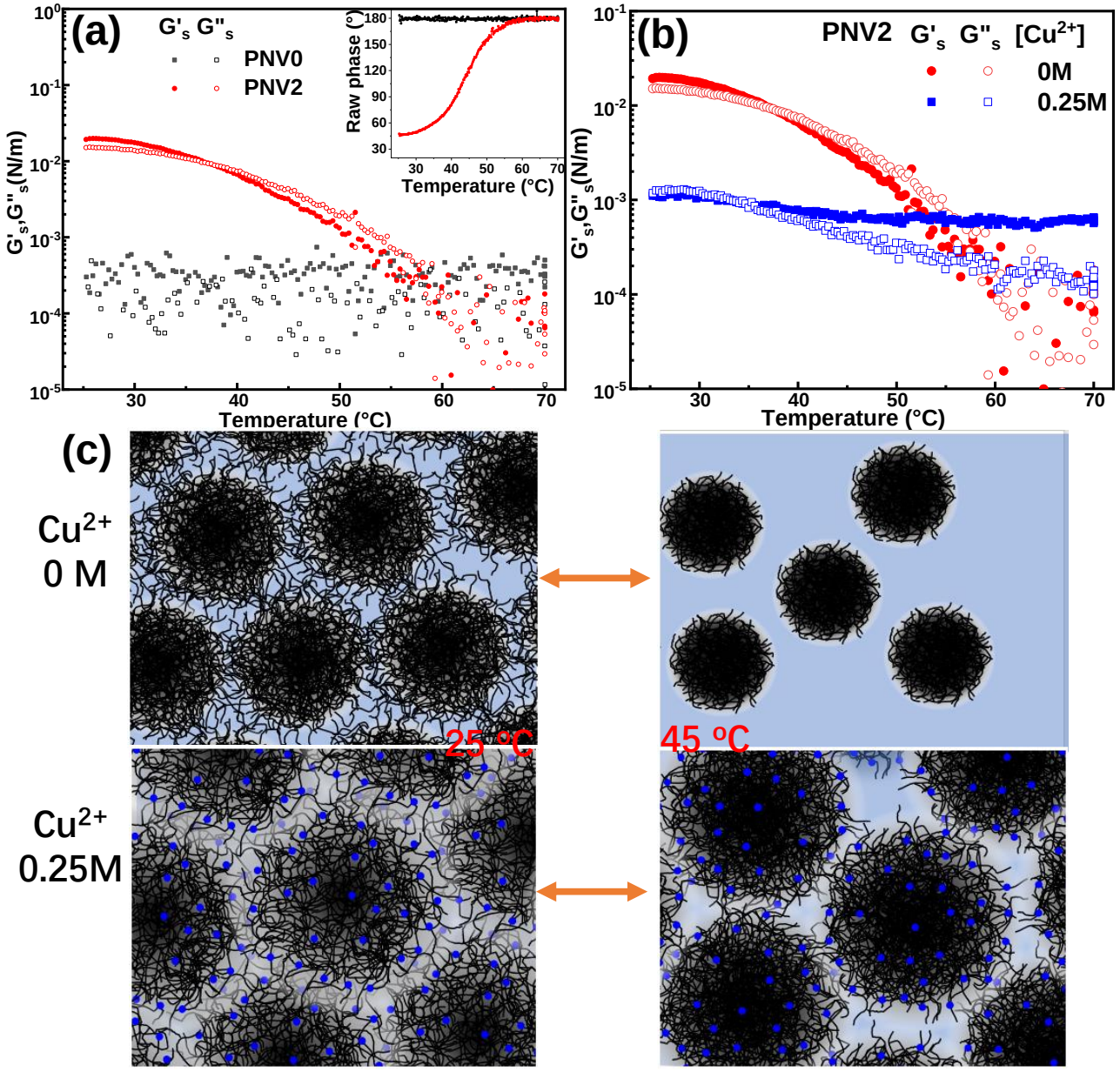

Figure 7. Surface shear viscoelasticity: storage modulus (G'_s, solid symbols) and loss modulus (G''_s, open symbols) as a function of temperature for microgels of PNV0 and PNV2 (a), and for microgels of PNV2 in the absence and presence of Cu^{2+}(0.25M)(b); (c) Schematic of a top view of the interactions between PNV2 microgels adsorbed at the air-water interface transitioning between 25 °C and 45 °C in the absence and presence of Cu^{2+}(0.25M).

Furthermore, the surface shear viscoelasticity of the microgels at air/water interface was measured using a Du Noüy ring (DDR) as a function of temperature (Fig. 6). Data of PNV0, which had a very weak foam stability (see Fig. 4a), was presented for comparison. As shown in Figure 6a, at 25 °C, a significant predominant elastic response with G'_s ~ 2.08 x 10^{-2} N/m and G''_s ~ 1.54 x 10^{-2} N/m was observed for PNV2, whereas the surface viscoelasticity (G'_s, G''_s) of PNV0 was nearly undetectable having largely discrete data due to its low torque in close proximity to the lower limit of torque sensor of rheometer. The high raw phase angle around 180° of PNV0 (see Fig.7a inset) also indicated the dominance of system inertia contribution over the interface contribution[47]. This difference on surface shear viscoelasticity between PNV0 and PNV2 is in good agreement with foam stability data (Fig.4a) as a robust interfacial film provides a better resistance against coalescence of bubbles. As temperature increased, the surface viscoelasticity experienced a gradual reduction, with the transition (i.e. G'_s-G''_s crossover) from solid-like ($G'_s > G''_s$) to liquid-like ($G'_s < G''_s$) response happened around the VPTT of the microgels(i.e. ~ 40 °C for PNV2). This responsive change in surface viscoelasticity strongly supports the “smart” feature of the thermo-responsive PNV-stabilized foams.

For the case of PNV2-Cu (0.25 M Cu^{2+}) that was demonstrated to be softer than PNV2, the microgel exhibited a lower surface viscoelasticity but a more gel-like behavior ($G'_s \approx G''_s$) (Fig.7b). This confirmed the increased softness

provided by Cu^{2+} complexation as demonstrated by SLS (Fig.3). Meanwhile, the thermo-responsive reduction of surface viscoelasticity was greatly mitigated in the PNV2-Cu with a much smaller G'_s(25 °C)/G'_s(70 °C) ratio (~1.68) than that of pure PNV2 (~300.1). This was well consistent with the weakened thermo-responsiveness of foams stabilized by Cu^{2+} complexed PNV2 microgels (Fig. 4b,c). This confirms that the responsive foam destabilization of PNV2 microgels was dominated by bubble coalescence as a result of weak shear viscoelasticity of the interfacial layer. However, Cu^{2+} complexation was able to guarantee the PNV microgels with a considerable surface shear elasticity to resist such bubble coalescence.

As schemed in Fig. 7c, at 25 °C, the swollen microgels with dangling polymer chains at the particle periphery are supposed to spread on the interface and overlap or entangle with each other to create a robust interfacial film, though a softer microgel (PNV2-Cu) can lower the surface viscoelasticity to a gel-like state. At 45 °C, PNV2 were shrunk into rigid particles with a lower volume occupying a smaller surface area, and transitioning the interfacial film to a liquid-like state. However, for PNV2-Cu, though the microgels were partially de-swelled but still had a lot of dangling polymer chains at particle periphery that kept strong chain entanglements and overlapping between neighboring microgels, thus maintaining a great surface viscoelasticity and hence the ultra-stability of foams.

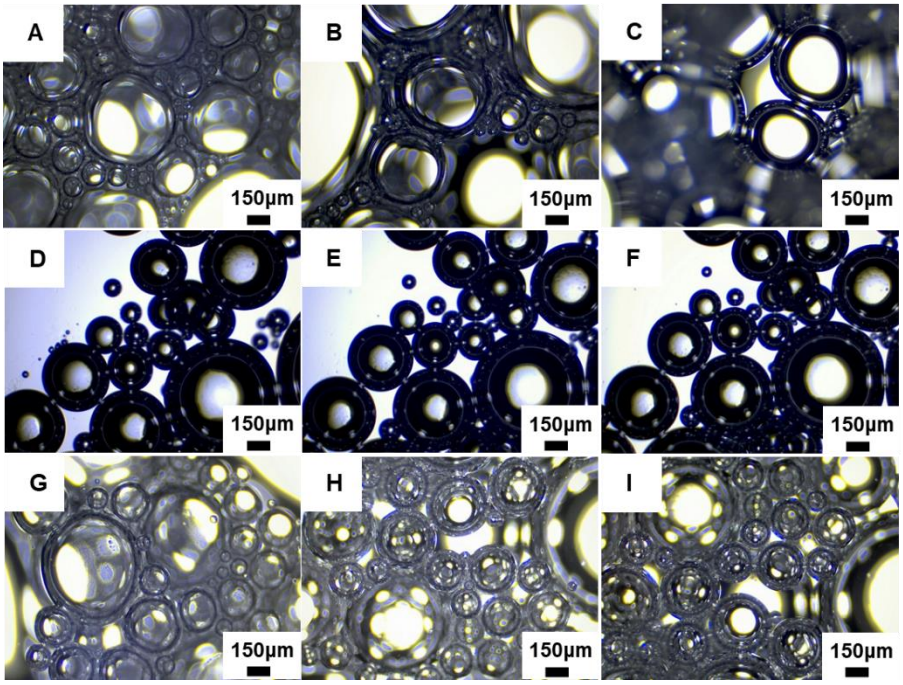

Figure 8. Image sequence of foam aging at t= 0, 10, 20 min after foam preparation of PNV2 (A-C), PNV2-Cu (0.25M Cu^{2+})(D-F) and SDS (G-I) at 25 ^{o}C.

In addition, the use of Cu^{2+} complexed PNV2 microgels as foam stabilizers had advantages over the others on keeping the interfacial films wet to reduce liquid drainage and/or drying as benefited from the superior swelling and the good solvation of Cu^{2+} ions. This was evidenced by the optical microscopic observation on the evolution of foam morphology with time at 25 ^{o}C (see Fig. 8). Upon aging, bubble shrinkage was observed in the PNV2 stabilized foam (Fig. 8A-C), with bubble size gradually reduced and bubble shape become crimped as a result of liquid drainage and coarsening. In contrast, the PNV2-Cu stabilized foam (Fig. 8D-F) exhibited a better stability, having no obvious rupture tendency for 20 minutes under the resolution of optical microscope. This is similar with the SDS-stabilized foam (Fig. 8G-I) but the SDS-stabilized foam was

lightly dried out as a result of liquid drainage. Such good stability of the PNV2-Cu stabilized foams was believed to be associated with the thick interfacial layer of ion complexed microgels surrounding the bubbles that had a good water retention ability and a strong mechanical property to resist coalescence/ coarsening.

3.4 Selective recovery of Cu^{2+} from mixed salt solutions

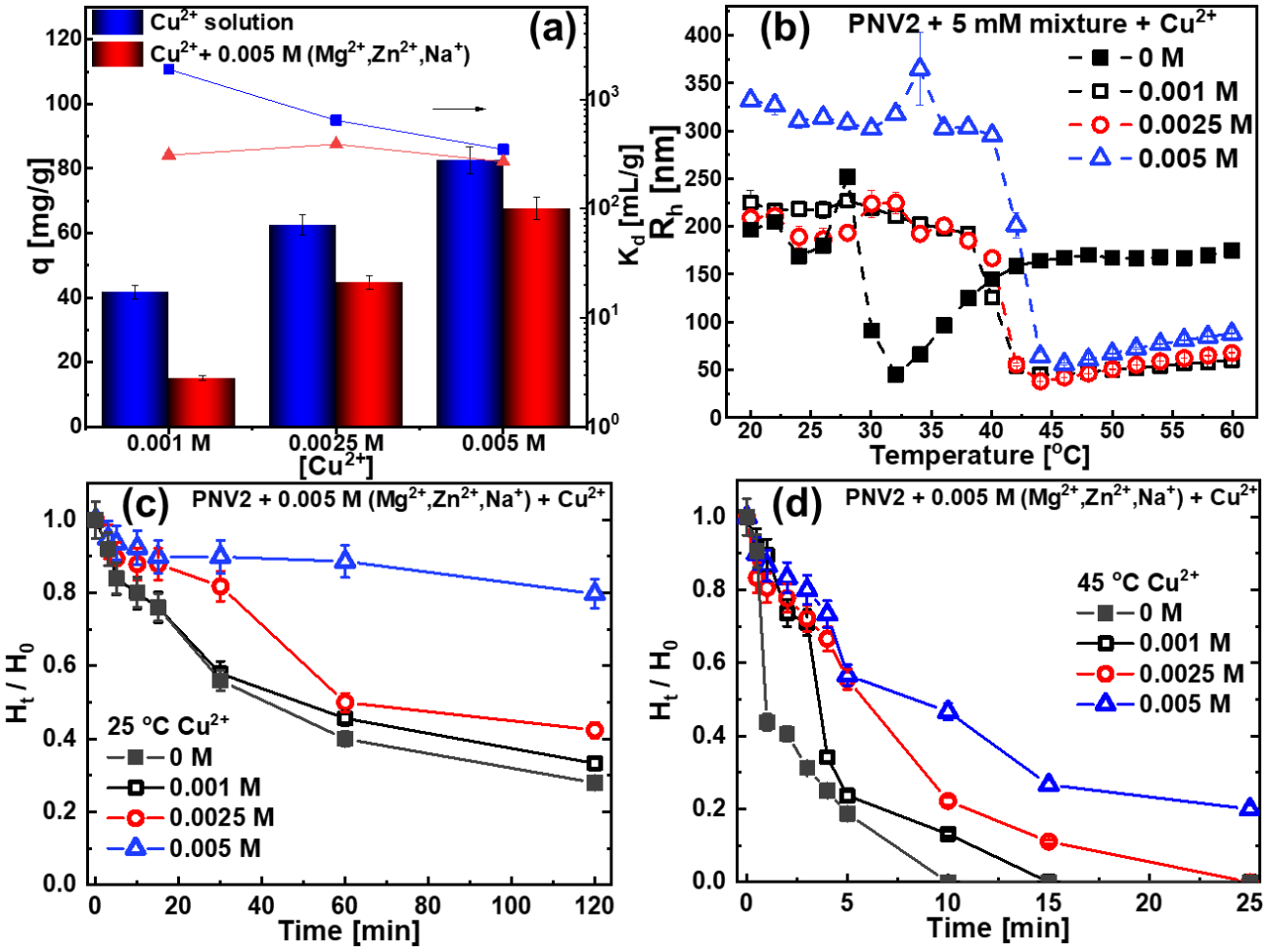

Figure 9. (a) Cu^{2+} sorption capacity *q* of PNV2 as a function of the initial Cu^{2+} concentration in $CuSO_4$ solutions and in mixed salt solutions; (b) temperature dependence of R_h of PNV2 in mixed salt solutions with varied Cu^{2+} concentrations; (c-d) relative foam height (H_t/H_0) as a function of time (c: 25 °C,

d: 45 °C) for PNV2 in mixed salt solutions with varied Cu^{2+} concentrations. The mixed salt solutions contained competitive ions of Mg^{2+}, Zn^{2+}, Na^{+} at a fixed concentration of 0.005 M.

In practical environment Cu^{2+} is often coexisting with competitive ions, to evaluate the selective recovery capacity of the as-prepared PNV2 microgel to Cu^{2+} from coexisting competitive ions, sorption experiments were conducted in salt solutions containing 0.005 M Mg^{2+}, Zn^{2+}, Na^{+}, mixing with Cu^{2+} at varied concentrations. The pure Cu^{2+} solutions at same concentrations were used as control sample. As shown in Fig. 9a, the PNV2 exhibited a good Cu^{2+} sorption capacity (e.g. q ~ 82.6 mg/g at 0.005 M Cu^{2+}), and the q experienced a reduction to some extent when multiple competitive ions were presented. However, the reduction was not that significant especially when the Cu^{2+} concentration was increased to the same level as the competitive ions, that is, only a small change from 82.6 mg/g to 67.7 mg/g at 0.005 M Cu^{2+}. Distribution coefficient, $K_d = (C_O - C_e)/C_e \cdot (V/m)$ with C_0, C_e the initial and equilibrium concentration of Cu^{2+}, V the volume of solution and m the mass of adsorbent, was also calculated to evaluate the sorption selectivity. The K_d also shows a reducing difference with increased Cu^{2+} concentration between solutions with and without competitive ions, equating to 2.68 x 10^2 and 3.09 x 10^2 mL/g at 0.005 M Cu^{2+} for the former and the later, respectively. Hence a good selectivity of the PNV2 microgel to Cu^{2+} from mixed salt solution was thus demonstrated. Such sorption capacity

and selectivity are sitting in the rank of high-level adsorbents when comparing to those containing nitrogen-based ligands as reported in the literature [1].

Moreover, the measurement of hydrodynamic radius (R_h) of the PNV2 microgel in mixed salt solutions containing 0.005 M Mg^{2+}, Zn^{2+}, Na^{+} plus Cu^{2+} with varied concentrations (Fig.9b) also indicates the good selectivity of particle swelling behavior to Cu^{2+}. In particular, in the absence of Cu^{2+}, the particle in mixed solution exhibited a VPTT around 28 ^{o}C, a negative shift from pure PNV2 as a result of weak Zn^{2+}-amide complexation (Fig. 2d) and an aggregation phenomenon above the VPTT as a result of charge screening effect. However, in the presence of Cu^{2+}, the particle aggregation above the VPTT was avoided and the VPTT was positively shifted with increased Cu^{2+} concentration to 43 ^{o}C at 0.005M Cu^{2+}, able to distinguish the particles before and after Cu^{2+} sorption. Note that the particle size decrement observed here in mixed solutions as compared to the pure system (Fig.2) is supposed to a result of the complex Hofmeister effect (i.e. “salt-out”) and osmotic effect of co-existing multi-ions[70]. This, however, does not affect the conclusion of the Cu^{2+} selectivity of the PNV2 microgel.

The good Cu^{2+} selectivity from mixed salt solutions was further confirmed by the foam tests conducted at both 25 ^{o}C and 45 ^{o}C. As shown in Fig. 9c,d, in the mixed solutions of 0.005 M Mg^{2+}, Zn^{2+}, Na^{+}, the presence of Cu^{2+} greatly enhanced the foam stability with foam height and foam life increased with increasing Cu^{2+} concentration, even though the foam stability was weakened to

some extent at 45 ^{o}C as a result of particle deswelling in the mixed solution.

In a word, Cu^{2+} was demonstrated to be selectively recoverable from wastewater containing multiple competitive ions via responsive flotation based on the as-prepared PNV2 microgel. Once the Cu^{2+} complexed microgels are potentially separated from aqueous environment with foams via flotation, the foams can be readily destabilized by heating up to the VPTT of the Cu^{2+} complexed microgel to recover the Cu^{2+}. The Cu^{2+} recovery is envisioned to be limited by the imidazole groups of the polymer. The proposed smart flotation strategy for “one-step” Cu^{2+} recovery is expected to overtake conventional water treatment techniques in terms of efficiency, environment friendliness, and ease of scale-up.

4. Conclusion

A thermosensitive and Cu^{2+} responsive poly (N-Isopropylacrylamide-co-Vinyl imidazole) (PNV2) microgel with a hydrodynamic radius of 334 $\pm$ 2.2 nm and a fuzziness of 37.2$\pm$ 7.9 nm has been successfully synthesized using a surfactant-free precipitation polymerization, as confirmed via a series of techniques. The VIM monomer at a feeding ratio of 20 wt% enhanced the swelling ratio of the pNIPAM-based microgel from 1.89 to 2.35 with a VPTT shift from ~32.5 ^{o}C to ~40 ^{o}C. The Cu^{2+}-imidazole complexation was demonstrated to further enhance the swelling of the PNV microgel by an order of 30-50 nm in particle radius for Cu^{2+} within 0.005 M and 0.25 M. The VPTT shift significantly

from ~40 °C to ~50 °C for 0.005 M Cu^{2+}, ~60 °C for 0.05 M Cu^{2+} and >> 60 °C for 0.25 M Cu^{2+}, and the swelling/deswelling was tuneable by Cu^{2+} concentration. A softer and more homogenous microstructure with a more perfect spherical shape of the Cu^{2+} complexed PNV microgels than pure PNV was demonstrated based on the particle form factor analysis via SLS and the fuzzy sphere model.

Thermo-responsive “smart” foams were readily stabilized by the PNV2 microgels with a ultra-stability below its VPTT while rapidly collapsed above the VPTT when the microgels deswelled. The Cu^{2+} complexation enabled a modulation of temperature responsiveness of the foams by Cu^{2+} concentration, able to maintain a good foam stability in high temperatures(e.g. a life time > 6 h at 45 °C with 0.25 M Cu^{2+}) whilst foams collapsed in solutions of competitive ions (e.g. ~2 min, ~10 min and ~15 min for Na^{+}, Mg^{2+}, Zn^{2+}, respectively), providing possibility for selective Cu^{2+} recovery via a responsive froth flotation.

The interfacial study at air-water interface confirmed a good surface activity of both the swollen and collapsed PNV microgels with a maximum particle diffusivity (~ 6.12×10^{-7} m^2s^{-1}) towards the interface around the VPTT. The Cu^{2+} complexation better increased the surface acitivity of the microgel and weakened the temperature dependence of the interfacial diffusivity. Meanwhile, the Cu^{2+} complexation increased the surface dilatational viscoelasticity and reduced the thermosensitivity, but still insufficient to fully hamper bubble coarsening. A significant reduction in surface shear elasticity across the VPTT of microgels, with a G'_s(25 °C)/G'_s(70 °C) ratio ~300.1, was demonstrated to be

the dominant reason in controlling the responsive foam destabilization. The overlapping and engtanglements of dangling chains between the ultra-soft and swollen Cu^{2+}-complexed PNV microgels was supposed to guarantee the great surface shear viscoelasticity, giving a G'_s(25 ^oC)/G'_s(70 ^oC) ratio ~1.68, and thus the ultra-stable foams at high temperatures.

Ultimately, the good Cu^{2+} selectivity of PNV2 microgel was well demonstrated in multi-component solutions mixing 0.005 M competitive ions Na^+, Mg^{2+}, Zn^{2+} with Cu^{2+} at varied concentrations. The PNV2 exhibited a good Cu^{2+} sorption capacity, ~ 82.6 mg/g and ~ 67.7 mg/g at 0.005 M Cu^{2+} in the absence and the presence of mixed competitive ions, respectively. The Cu^{2+} tunnable particle swelling was maintained in the mixed salt solutions though the VPTT value was counterbalanced by Zn^{2+}-amide complexation. The Cu^{2+} tunnable foam stabillity was also reserved in the mixed salt solutions.

Overall, this study provides a new concept of using ion-complexation to regulate the stimuli-responsiveness of microgels and hence its stabilized foams/emulsions. The obtained results pave foundations to develop a responsive flotation for selective Cu^{2+} recovery in one step, which promisingly owns advantages over conventional treatment techniques on efficiency, circular economy and simplicity, etc.

Acknowledgement

Dr Olli-Ville Laukkanen and Dr Carlos G. Lopez are acknowledged for technical

supports on tensiometry and SLS measurements. This work was financially supported by the European Union's Horizon 2020 research and innovation programme under the Marie Skłodowska-Curie Grant Agreement No. 844286(M4WASTE), the National Natural Science Foundation of China (21903015; 22172028;22111530080), the Natural Science Foundation of Fujian Province of China (2020J01145), the Fujian Provincial Health Education Joint Research Project (WKJ2016-2-11), and the Award Program of Fujian Minjiang Scholar Professorship (2018). W.R. greatly acknowledges the Deutsche Forschungsgemeinschaft for the financial support of SFB 985 "Functional Microgels and Microgel Systems" (Project B8).

Corresponding Author

H.Z. Email : zhang@pc.rwth-aachen.de

References

[1] J. Liu, D.H. Su, J.R. Yao, Y.F. Huang, Z.Z. Shao, X. Chen, Soy protein-based polyethylenimine hydrogel and its high selectivity for copper ion removal in wastewater treatment, J Mater Chem A 5 (2017) 4163-4171.

[2] H.G. Zhang, Y.K. Kim, T.N. Hunter, A.P. Brown, J.W. Lee, D. Harbottle, Organically modified clay with potassium copper hexacyanoferrate for enhanced Cs+ adsorption capacity and selective recovery by flotation, J Mater Chem A 5 (2017) 15130-15143.

[3] P. Pulkkinen, J. Shan, K. Leppanen, A. Kansakoski, A. Laiho, M. Jarn, H. Tenhu, Poly(ethylene imine) and Tetraethylenepentamine as Protecting Agents for Metallic Copper Nanoparticles, Acs Appl Mater Inter 1 (2009) 519-525.

[4] C.B. Tabelin, I. Park, T. Phengsaart, S. Jeon, M. Villacorte-Tabelin, D. Alonzo, K. Yoo, M. Ito, N. Hiroyoshi, Copper and critical metals production from porphyry ores and E-wastes: A review of resource availability, processing/recycling challenges, socio-environmental aspects, and sustainability issues, Resour Conserv Recy 170 (2021).

[5] T. Tatsuhara, T. Arima, T. Igarashi, C.B. Tabelin, Combined neutralization-adsorption system for the disposal of

hydrothermally altered excavated rock producing acidic leachate with hazardous elements, Eng Geol 139 (2012) 76-84.
[6] S. Tomiyama, T. Igarashi, C.B. Tabelin, P. Tangviroon, H. Ii, Modeling of the groundwater flow system in excavated areas of an abandoned mine, J Contam Hydrol 230 (2020).
[7] C.B. Tabelin, T. Igarashi, M. Villacorte-Tabelin, I. Park, E.M. Opiso, M. Ito, N. Hiroyoshi, Arsenic, selenium, boron, lead, cadmium, copper, and zinc in naturally contaminated rocks: A review of their sources, modes of enrichment, mechanisms of release, and mitigation strategies, Sci Total Environ 645 (2018) 1522-1553.
[8] T. Igarashi, P.S. Herrera, H. Uchiyama, H. Miyamae, N. Iyatomi, K. Hashimoto, C.B. Tabelin, The two-step neutralization ferrite-formation process for sustainable acid mine drainage treatment: Removal of copper, zinc and arsenic, and the influence of coexisting ions on ferritization, Sci Total Environ 715 (2020).
[9] S. Tomiyama, T. Igarashi, C.B. Tabelin, P. Tangviroon, H. Ii, Acid mine drainage sources and hydrogeochemistry at the Yatani mine, Yamagata, Japan: A geochemical and isotopic study, J Contam Hydrol 225 (2019).
[10] M.S. Liu, E. Almatrafi, Y. Zhang, P. Xu, B. Song, C.Y. Zhou, G.M. Zeng, Y. Zhu, A critical review of biochar-based materials for the remediation of heavy metal contaminated environment: Applications and practical evaluations, Sci Total Environ 806 (2022).
[11] S. Jeon, C.B. Tabelin, H. Takahashi, I. Park, M. Ito, N. Hiroyoshi, Interference of coexisting copper and aluminum on the ammonium thiosulfate leaching of gold from printed circuit boards of waste mobile phones, Waste Manage 81 (2018) 148-156.
[12] J. Lu, P.K. Mishra, T.N. Hunter, F. Yang, Z. Lu, D. Harbottle, Z. Xu, Functionalization of mesoporous carbons derived from pomelo peel as capacitive electrodes for preferential removal/recovery of copper and lead from contaminated water, Chem Eng J (2022) 134508.
[13] C.B. Tabelin, V.J.T. Resabal, I. Park, M.G.B. Villanueva, S. Choi, R. Ebio, P.J. Cabural, M. Villacorte-Tabelin, A. Orbecido, R.D. Alorro, S. Jeon, M. Ito, N. Hiroyoshi, Repurposing of aluminum scrap into magnetic Al-0/ZVI bimetallic materials: Two-stage mechanical-chemical synthesis and characterization of products, J Clean Prod 317 (2021).
[14] H.G. Zhang, S. Tangparitkul, B. Hendry, J. Harper, Y.K. Kim, T.N. Hunter, J.W. Lee, D. Harbottle, Selective separation of cesium contaminated clays from pristine clays by flotation, Chem Eng J 355 (2019) 797-804.
[15] H. Polat, D. Erdogan, Heavy metal removal from waste waters by ion flotation, J Hazard Mater 148 (2007) 267-273.
[16] F.S. Hoseinian, M. Irannajad, A.J. Nooshabadi, Ion flotation for removal of Ni(II) and Zn(II) ions from wastewaters, Int J Miner Process 143 (2015) 131-137.
[17] A.C. Martinez, E. Rio, G. Delon, A. Saint-Jalmes, D. Langevin, B.P. Binks, On the origin of the remarkable stability of aqueous foams stabilised by nanoparticles: link with microscopic surface properties, Soft matter 4 (2008) 1531-1535.
[18] A.-L. Fameau, A. Carl, A. Saint-Jalmes, R. von Klitzing, Responsive Aqueous Foams, ChemPhysChem 16 (2015) 66-75.
[19] S. Tsuji, H. Kawaguchi, Thermosensitive Pickering Emulsion Stabilized by Poly(N-isopropylacrylamide)-Carrying Particles, Langmuir 24 (2008) 3300-3305.
[20] W. Richtering, Responsive Emulsions Stabilized by Stimuli-Sensitive Microgels: Emulsions with Special Non-Pickering Properties, Langmuir 28 (2012) 17218-17229.
[21] Y. Horiguchi, H. Kawakita, K. Ohto, S. Morisada, Temperature-responsive Pickering foams stabilized by poly(N-isopropylacrylamide) nanogels, Adv Powder Technol 29 (2018) 266-272.
[22] R.H. Pelton, P. Chibante, Preparation of aqueous latices with N-isopropylacrylamide, Colloids and surfaces 20 (1986) 247-256.

[23] S. Meyer, W. Richtering, Influence of Polymerization Conditions on the Structure of Temperature-Sensitive Poly(N-isopropylacrylamide) Microgels, Macromolecules 38 (2005) 1517-1519.
[24] M. Heskins, J.E. Guillet, Solution Properties of Poly(N-isopropylacrylamide), Journal of Macromolecular Science: Part A - Chemistry 2 (1968) 1441-1455.
[25] J. Rika, M. Meewes, R. Nyffenegger, T. Binkert, Intermolecular and intramolecular solubilization: Collapse and expansion of a polymer chain in surfactant solutions, Physical Review Letters 65 (1990) 657-660.
[26] H.G. Schild, D.A. Tirrell, Interaction of poly(N-isopropylacrylamide) with sodium n-alkyl sulfates in aqueous solution, Langmuir 7 (1991) 665-671.
[27] H.G. Schild, Poly(N-isopropylacrylamide): experiment, theory and application, Progress in Polymer Science 17 (1992) 163-249.
[28] W. Saito, O. Mori, Y. Ikeo, M. Kawaguchi, T. Imae, T. Kato, Surface Pressure, Ellipsometric, and Atomic Force Microscopic Study of Poly(N-isopropylacrylamide) Film at the Air-Water Interface, Macromolecules 28 (1995) 7945-7946.
[29] B. Sierra-Martin, J.R. Retama, M. Laurenti, A. Fernández Barbero, E. López Cabarcos, Structure and polymer dynamics within PNIPAM-based microgel particles, Advances in Colloid and Interface Science 205 (2014) 113-123.
[30] Y. Yang, M. Zhang, L.S. Sha, P. Lu, M. Wu, "Bottom-Up" Assembly of Nanocellulose Microgels as Stabilizer for Pickering Foam Forming, Biomacromolecules 22 (2021) 3960-3970.
[31] T. Ngai, H. Auweter, S.H. Behrens, Environmental responsiveness of microgel particles and particle-stabilized emulsions, Macromolecules 39 (2006) 8171-8177.
[32] B. Brugger, W. Richtering, Emulsions stabilized by stimuli-sensitive poly (N-isopropylacrylamide)-co-methacrylic acid polymers: Microgels versus low molecular weight polymers, Langmuir 24 (2008) 7769-7777.
[33] S. Fujii, E.S. Read, B.P. Binks, S.P. Armes, Stimulus-responsive emulsifiers based on nanocomposite microgel particles, Advanced Materials 17 (2005) 1014-1018.
[34] S. Fujii, S.P. Armes, B.P. Binks, R. Murakami, Stimulus-responsive particulate emulsifiers based on lightly cross-linked Poly (4-vinylpyridine)– silica nanocomposite microgels, Langmuir 22 (2006) 6818-6825.
[35] S. Bochenek, A. Scotti, W. Ogieglo, M.A. Fernandez-Rodriguez, M.F. Schulte, R.A. Gumerov, N.V. Bushuev, I.I. Potemkin, M. Wessling, L. Isa, W. Richtering, Effect of the 3D Swelling of Microgels on Their 2D Phase Behavior at the Liquid-Liquid Interface, Langmuir 35 (2019) 16780-16792.
[36] S. Bochenek, A. Scotti, W. Richtering, Temperature-sensitive soft microgels at interfaces: air-water versus oil-water, Soft Matter 17 (2021) 976-988.
[37] J. Harrer, M. Rey, S. Ciarella, H. Lowen, L.M.C. Janssen, N. Vogel, Stimuli-Responsive Behavior of PNiPAm Microgels under Interfacial Confinement, Langmuir 35 (2019) 10512-10521.
[38] V. Schmitt, V. Ravaine, Surface compaction versus stretching in Pickering emulsions stabilised by microgels, Curr Opin Colloid In 18 (2013) 532-541.
[39] R. Kanazawa, K. Mori, H. Tokuyama, S. Sakohara, Preparation of thermosensitive microgel adsorbent for quick adsorption of heavy metal ions by a temperature change, J Chem Eng Jpn 37 (2004) 804-807.
[40] X.J. Zhou, J.J. Nie, B.Y. Du, Functionalized Ionic Microgel Sensor Array for Colorimetric Detection and Discrimination of Metal Ions, Acs Appl Mater Inter 9 (2017) 20913-20921.
[41] Y.Q. Liu, X.J. Ju, X.Q. Pu, S. Wen, W.Y. Liu, Z. Liu, W. Wang, R. Xie, L.Y. Chu, Visual detection of trace lead(II) using a forward osmosis-driven device loaded with ion-responsive nanogels, J Hazard Mater 404 (2021).
[42] J. Peng, N. Zhao, S. Lin, W. Wang, M.J. Zhang, Y.Y. Su, R. Xie, X.J. Ju, Z. Liu, L.Y. Chu, Smart microfluidic analogue of Wheatstone-bridge for real-time continuous detection with ultrasensitivity and wide dynamic range, Chem Eng J 407 (2021).

[43] J. Adusei-Gyamfi, B. Ouddane, L. Rietveld, J.-P. Cornard, J. Criquet, Natural organic matter-cations complexation and its impact on water treatment: A critical review, Water research 160 (2019) 130-147.
[44] E. Farkas, D. Batka, E. Csapo, P. Buglyo, W. Haase, D. Sanna, Synthesis and characterization of Cu2+, Ni2+ and Zn2+ binding capability of some amino- and imidazole hydroxamic acids: Effects of substitution of side chain amino-N for imidazole-N or hydroxamic-N-H for -N-CH3 on metal complexation, Polyhedron 26 (2007) 543-554.
[45] W. Burchard, W. Richtering, Dynamic Light-Scattering from Polymer-Solutions, Prog Coll Pol Sci S 80 (1989) 151-163.
[46] M. Stieger, W. Richtering, J.S. Pedersen, P. Lindner, Small-angle neutron scattering study of structural changes in temperature sensitive microgel colloids, The Journal of chemical physics 120 (2004) 6197-6206.
[47] S. Vandebril, A. Franck, G.G. Fuller, P. Moldenaers, J. Vermant, A double wall-ring geometry for interfacial shear rheometry, Rheologica Acta 49 (2010) 131-144.
[48] H.G. Zhang, K. Yu, O.J. Cayre, D. Harbottle, Interfacial Particle Dynamics: One and Two Step Yielding in Colloidal Glass, Langmuir 32 (2016) 13472-13481.
[49] X. Zhou, Y. Zhou, J. Nie, Z. Ji, J. Xu, X. Zhang, B. Du, Thermosensitive ionic microgels via surfactant-free emulsion copolymerization and in situ quaternization cross-linking, ACS applied materials & interfaces 6 (2014) 4498-4513.
[50] Q. Wang, Y. Zhao, H. Xu, X. Yang, Y. Yang, Thermosensitive phase transition kinetics of poly(N-isopropylacryl amide-co-acrylamide) microgel aqueous dispersions, Journal of Applied Polymer Science 113 (2009) 321-326.
[51] B.R. Saunders, H.M. Crowther, G.E. Morris, S.J. Mears, T. Cosgrove, B. Vincent, Factors affecting the swelling of poly(N-isopropylacrylamide) microgel particles: fundamental and commercial implications, Colloids and Surfaces A: Physicochemical and Engineering Aspects 149 (1999) 57-64.
[52] S. Schachschal, H.-J. Adler, A. Pich, S. Wetzel, A. Matura, K.-H. van Pee, Encapsulation of enzymes in microgels by polymerization/cross-linking in aqueous droplets, Colloid and Polymer Science 289 (2011) 693-698.
[53] R.H. Pelton, H.M. Pelton, A. Morphesis, R.L. Rowell, Particle sizes and electrophoretic mobilities of poly (N-isopropylacrylamide) latex, Langmuir 5 (1989) 816-818.
[54] F.A. Plamper, W. Richtering, Functional microgels and microgel systems, Accounts of chemical research 50 (2017) 131-140.
[55] M.E.A. Ali, F.M. Hassan, X. Feng, Improving the performance of TFC membranes via chelation and surface reaction: applications in water desalination, Journal of Materials Chemistry A 4 (2016) 6620-6629.
[56] Z. Liu, Y. Hu, C. Liu, Z. Zhou, Surface-independent one-pot chelation of copper ions onto filtration membranes to provide antibacterial properties, Chemical Communications 52 (2016) 12245-12248.
[57] C.B. Tabelin, M. Silwamba, F.C. Paglinawan, A.J.S. Mondejar, H.G. Duc, V.J. Resabal, E.M. Opiso, T. Igarashi, S. Tomiyama, M. Ito, N. Hiroyoshi, M. Villacorte-Tabelin, Solid-phase partitioning and release-retention mechanisms of copper, lead, zinc and arsenic in soils impacted by artisanal and small-scale gold mining (ASGM) activities, Chemosphere 260 (2020).
[58] X.L. Li, I. Park, C.B. Tabelin, K. Naruwa, T. Goda, C. Harada, S. Jeon, M. Ito, N. Hiroyoshi, Enhanced pyrite passivation by carrier-microencapsulation using Fe-catechol and Ti-catechol complexes, J Hazard Mater 416 (2021).
[59] I. Park, C.B. Tabelin, K. Seno, S. Jeon, M. Ito, N. Hiroyoshi, Simultaneous suppression of acid mine drainage formation and arsenic release by Carrier-microencapsulation using aluminum-catecholate complexes, Chemosphere 205 (2018) 414-425.
[60] E. Daly, B.R. Saunders, A study of the effect of electrolyte on the swelling and stability of poly(N-isopropylacrylamide) microgel dispersions, Langmuir 16 (2000) 5546-5552.
[61] H. Senff, W. Richtering, Temperature sensitive microgel suspensions: Colloidal phase behavior and rheology of soft spheres, J Chem Phys 111 (1999) 1705-1711.
[62] J.L. Sanchez-Salvador, M.C. Monte, C. Negro, W. Batchelor, G. Garnier, A. Blanco, Simplification of gel point

characterization of cellulose nano and microfiber suspensions, Cellulose 28 (2021) 6995-7006.
[63] H. Zhang, K. Yu, O.J. Cayre, D. Harbottle, Interfacial particle dynamics: one and two step yielding in colloidal glass, Langmuir 32 (2016) 13472-13481.
[64] Z.S. Pour, M. Ghaemy, Removal of dyes and heavy metal ions from water by magnetic hydrogel beads based on poly(vinyl alcohol)/carboxymethyl starch-g-poly(vinyl imidazole), Rsc Adv 5 (2015) 64106-64118.
[65] Z. Li, K. Geisel, W. Richtering, T. Ngai, Poly (N-isopropylacrylamide) microgels at the oil–water interface: adsorption kinetics, Soft Matter 9 (2013) 9939-9946.
[66] R.A. Gumerov, A.A. Rudov, W. Richtering, M. Mo¨ller, I.I. Potemkin, Amphiphilic arborescent copolymers and microgels: from unimolecular micelles in a selective solvent to the stable monolayers of variable density and nanostructure at a liquid Interface, ACS applied materials & interfaces 9 (2017) 31302-31316.
[67] K. Yu, B. Li, H. Zhang, Z. Wang, W. Zhang, D. Wang, H. Xu, D. Harbottle, J. Wang, J. Pan, Critical role of nanocomposites at air-water interface: from aqueous foams to foam-based lightweight functional materials, Chemical Engineering Journal (2021) 129121.
[68] T.B.J. Blijdenstein, R.A. Ganzevles, P.W.N. De Groot, S.D. Stoyanov, On the link between surface rheology and foam disproportionation in mixed hydrophobin HFBII and whey protein systems, Colloids and Surfaces A: Physicochemical and Engineering Aspects 438 (2013) 13-20.
[69] N.J. Alvarez, S.L. Anna, T. Saigal, R.D. Tilton, L.M. Walker, Interfacial dynamics and rheology of polymer-grafted nanoparticles at air–water and xylene–water interfaces, Langmuir 28 (2012) 8052-8063.
[70] W.S.P. Carvalho, C. Lee, Y.N. Zhang, A. Czarnecki, M.J. Serpe, Probing the response of poly (N-isopropylacrylamide) microgels to solutions of various salts using etalons, J Colloid Interf Sci 585 (2021) 195-204.